Interacting Artificial Surf Reefs

Le Hai Trung

TUDelft

Technische Universiteit Delft

Interacting Artificial Surf Reefs

MSc Thesis

Lê Hai Trung

Delft, 2006

Graduation committee

Prof.dr.ir. M. J. F. STIVE

Dr.ir. H.L. FONTIJN

Dr.ir. P.J. VISSER

Dr.ir. A.J.H.M. RENIERS

Dr.ir. I. CÁCERES

This thesis has been partly inspired by the article "Channel width influence on an Artificial Surf Reef" that is being finished at this moment from which I am one of the co-authors.

Acknowledgements

I wish to express my gratitude to all those who gave me possibilities to complete this thesis. I would like to thank my supervisors: prof. dr. ir. M.J.F. Stive, dr. ir. H.L. Fontijn, dr. ir. P.J. Visser, dr. ir. A.J.H.M. Reniers and dr. I. Cáceres for their supports and advices. Particularly Ad for giving me the chance to experience waves (they are never monochromatic) and Iván for sharing your time and enthusiasm to make me feel like working everyday.

I would like to acknowledge the helpful contributions which the staff of the Fluid Mechanics Laboratory offered me through the last months. I also want to thank Martijn Henriquez for the patient time and giving advice.

Delft, November 2006.

Lê Hải Trung.

Abstract

Wave surfing is existing and becoming more attractive in the Netherlands. However natural wave conditions are not suited to encourage the sport. To improve the surf conditions of the local waves, Artificial Surf Reefs are potential solutions. As a part of intentions to optimise the design of Artificial Surf Reefs, this thesis is aimed at gaining insight into the wave-induced circulations and the wave-current interactions around an artificial reef. Impacts of the channel width on these processes were assessed by varying the width of the channel. Several surf-ability parameters were measured or observed to verify the performance of the proposed design. The surface currents on either side of the reef show a decrease in intensities and dimensions resulting in less intense wave-current interactions around the structure. It was found that rip currents with a Froude number smaller than 0.1 do not cause negative impact on the breaker shapes.

Contents

Chapter 1

Introduction

1.1 Surfing

"Surfing is a surface water sport in which the participant is carried by a breaking wave on a surfboard" (Wikipedia.org, 2006). The shape and the quality of breaking waves are influenced by several factors including the bathymetry of the surf break, the swell, the wind conditions and the tide. These factors are unique for each surf break (spot). However, surfers all share a desire to ride "hollow" waves.

No one can tell when the sport was originated it could be far back in time before Captain Cook witnessed surfing in Hawaii in the late 1770s. In the 19th century, after the Europeans arrived, the sport was discouraged. Surfing revived and developed in the 20th century. Now surfing is not only a sport but a way of life. The surf community has been increasing and spreading all over the world. In contrast, the number of natural surf breaks is to be limited.

1.2 Artificial Surf Reef

The idea of creating artificial surf breaks has been initiated and implemented in several places from Australia to America. An Artificial Surf Reef (hereafter, denoted as ASR) is a man-made, underwater structure like a submerged breakwater aimed to improve surf conditions. Moreover ASRs are quite often considered multi-purpose structures for coastal protection and marine biology and to benefit the local economic through tourism.

Cable Station reef, constructed in 1999 in Western Australia, is known as the first Artificial Surf Reef anywhere in the world. It was constructed with granite rock producing both left and right breaks. Observation shows that Cable Station reef is now performing well, increasing the number of surfable days (PATTIARATCHI, 2003).
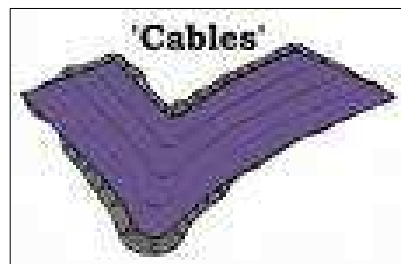
Figure 1.1 – Cable Station, Australia.

Another ASR was built at the Gold Coast, Australia as a multi-purpose structure maintaining and stabilising sand nourishment and improving local surfing condition (TURNER, et al., 2001). Numerical and physical simulation combining the effects of tides, wave heights and directions were performed to develop the reef to enhance surf conditions. The reef was made up of 300 sandbags of different sizes and shapes and costed 2 million US dollars.

Figure 1.2 – Gold Coast Reef, Australia.

Several other ASRs have been built like Mount Maunganui, New Zeeland, and Pratt's Reef in California, US. The great demand for surf breaks call for scientific and engineering studies and makes ASR a popular topic. The evolving knowledge concerning ASRs offers the opportunity of having surf-able waves in different locations around the world. Recently, at the Delft University of Technology, several relevant studies have been conducted. Some reef shapes have been designed by means of numerical computations and then verified with physical experiments.

HENRIQUEZ (2004) studied essential reef properties and then optimised the reef shape for varying wave conditions. Combining numerical and physical models, two important topographic features were found that greatly affect the peel angle: the angle enclosed by the offshore wave direction and the depth contour of the reef in the vicinity of wave breaking, the so called reef angle; and the relative depth at which the reef starts. Besides, numerical study showed that the reef performs best when the tip of the reef is relatively sharp. The numerical study was verified with a physical experiment. Laboratory measurements indicated that the breaker shapes are obviously affected by the water depth over the reef crest. In addition, wave-driven currents over and around the reef can be a dominant factor controlling the surf-ability of the breaking waves.

Later on, VAN ETTINGER (2005) designed an ASR, which includes two mirrored parts separated by a channel, specifically for Dutch swell conditions. During the design process, both waves and wave-driven currents were taken into account to optimise surf condition. The reef geometric shape was chosen upon a certain requirement of surf-ability parameters such as peel angle, breaker wave height and breaker shape. With numerical studies, the width of the channel was found to influence the wave-induced current pattern around the reef. The findings could be basically

Figure 1.3 – ASR model designed by VAN ETTINGER (2005).

translated as: by decreasing the width, the channel current velocity increases while the rip currents at the end of reef decrease; at a certain value of the channel width, the rip current no longer exists in the channel, and the rip currents through the breakers increase again.

The prototype shape of the reef was then scaled down to a physical model in a wave basin to verify the numerical predictions and obtain current velocity distributions as well as surf-ability parameters. With the design wave condition, the reef performed well producing plunging waves on both parts. Differences between numerical prediction and measured data were however recognised. Based on the existing design, a study on surf-ability of an ASR under irregular waves typically found at Scheveningen, the Netherlands was conducted by

OVER in 2006. The number of surf-able waves per year for waves coming from directions $240^0 - 270^0$ was estimated with respect to the presence of the tide.

Wave-driven currents can cause difficulties for surfers to maintain their positions or paddle back to the take-off zone. Rip currents can also flow through the breaker zone reducing the surf-ability of the waves and influence surrounding morphology. If the crest of the concerning reef is: (i) narrow; (ii) detached from the shoreline; (iii) fully submerged; and (iv) smooth with low frictional resistance, this ASR hence may experience strong wave-driven current flows (SYMONDS and BLACK, 2001). To optimise the reef design, proper understanding of wave-induced currents around an ASR is essential for the performance with respect to surfing. Further researches on this topic are encouraged.

1.3 Objectives

The study is aimed at finding the relation between the wave-induced current pattern around an ASR and the width of the channel in the middle of the reef, denoted as W_{RC}. In order to attain the main study objectives, several sub-objectives need to be achieved alternatively:

1. Understand the behaviour of the wave-induced currents at the ASR with different rip channel widths;

2. Investigate the wave-current interactions around the reef and the corresponding impacts on breaking waves;

3. Assess the surf conditions provided by the existing reef by measuring a number of surf-ability parameters.

1.4 Outline of the thesis

Following this introductory section, Chapter 2 describes the surf reef designed by VAN ETTINGER (2005). First, a number of design requirements are introduced and then the reef shape and its main geometric parameters are described. The chapter ends with a discussion on the wave-induced current pattern around an ASR.

The experimental set-up is presented in Chapter 3 with three main sections: instruments, test conditions and measurement procedure. The first section describes the main instruments used during the experiment to record water surface elevations and current velocities. Test conditions are detailed in the second section. The last section describes standard procedures of how the tests are conducted in the experiment.

Measured results including wave height distributions and velocity distributions are visualised by figures and graphs in Chapter 4.

In chapter 5 the experimental results presented in Chapter 4 are discussed.

Conclusions and recommendations are given in Chapter 6.

Appendix A sums the wave parameters of different conditions which were generated during the measurements. In Appendix B the positions of the different devices and the acquired data for the different experiments are tabulated. Finally an example of wave number and wave frequency calculation is presented in Appendix C.

Chapter 2

The reef design

Wave-driven currents around a surf break can negatively affect the surf-ability of the break or help the surfers paddle out to the breaker zone to catch a new wave. On a conventional artificial surf reef, it was shown that the rip currents can negatively affect about 20% of the wave rides (Henriquez, 2004). Van Ettinger (2005) designed the reef using the concept of an integral artificial surf reef which was first introduced in the design of the Gold Coast Reef in Australia. In the Gold Coast Reef, a channel in the middle of the reef was designed in order "to eliminate wave interference between the segments on the take-off zones; to provide sufficient wave crest length to develop a proper peak at the take-off and as a paddling channel to give surfers access to the break during moderate and large wave conditions" (Black and Mead, 2001). Van Ettinger created the rip channel in the middle of the reef in order to minimise the rip currents at either side of the reef. The design process was initiated by a set of requirements that can be found in the following section, which was partly rewritten from Van Ettinger (2005).

2.1 Required surfability parameters

Van Ettinger used several numerical models to design a surf reef for Dutch swell conditions. The design was generally dominated by the demanding surfability parameters. The typical North Sea wave condition experienced in the Netherlands on a good surfing day was modelled with bi-chromatic wave with a group period of 56 seconds. The offshore wave height is 1.5 m corresponding to the biggest wave in the group of seven waves. Definitions of surfability parameters can be found in studies of Henriquez (2004) and Van Ettinger (2005). Here only the required values of those surfability parameters are introduced. The selected surfer skill was not less than 5 in the 1-10 scale of surfing difficulty, which is primarily dependent on wave height, peel angle and wave steepness at the breakpoint (Hutt et al., 1998). The surfer skill was accordingly translated into a minimum peel angle of 40^0 for the design wave condition. A steep, plunging wave face was expected resulting in a minimum Iribarren number (ξ_b) (Battjes, 1974) of 0.4. Because of the relatively small offshore wave height, the waves should not break in a too plunging manner which would be difficult to surf. An Iribarren number ranging between 0.7 and 0.9 is therefore expected along the wave rides to provide suitable breaking shapes for surfing. At the start of the wave rides a value of 0.7 was however preferred for the take-off. The wave height (H_b) was required to be greater than the value of the offshore wave height (H_0). The main objective of the design was to optimise the surf conditions, therefore the rip currents through the breakers need to be minimised. Table 2.1 quantitatively summarises the required surf-ability parameters.

Table 2.1 – Design requirements.

Surf-ability parameter	Condition	Unit
Peel angle α_p	$40 \leq \alpha_p \leq 50$	[deg]
Iribarren number at take–off ξ_b	0.7	[-]
Iribarren number along wave ride ξ_b	$0.7 \div 0.9$	[-]
Wave height along wave ride H_b	$H_b \geq H_0$	[m]
Rip currents	minimized	[m/s]

2.2 The reef shape

The size and the shape of the reef were optimised through an extensive trial and error process with means of numerical models to satisfy the requirements listed in Table 2.1. The final reef consists of two parts separated by a channel. The reef shape and its characteristic parameters are illustrated in Figure 2.1.
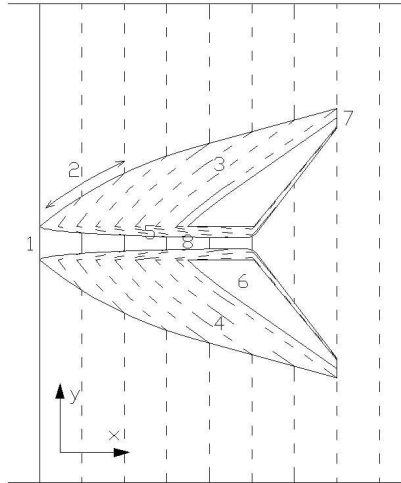
Figure 2.1 – The artificial surfing reef design.

As indicated in Figure 2.1, there are eight design features found to control the surf-ability and the wave-driven currents of the artificial surf reef. They are presented as follows with dimensions in prototype:

1. The reef was designed to start at a water depth of 6 m to give the longest possible wave ride;

2. The offshore tip has a certain curvature determined by a radius of 100 meter. Waves at the offshore tip barely refract, therefore a gentler slope of 1:9 is recognised. A relatively low breaking intensity is thus attained allowing an easy take-off;

3. The reef main slope at both sides is 1:7;

6

4. A reef angle of 55^0 was selected to satisfy the demanded peel angle;

5. The inner slope of the channel is 1:1;

6. The reef crest is 1.5 m below the still water level to ensure that the smallest wave in the group still breaks on the structure;

7. The back of the reef is cut to make the depth behind the reef as large as possible what is believed to weaken rip currents;

8. The width of the channel controls the flow of water through the channel and thus relieves the momentum from other currents. A channel width of 10 m was chosen in order to produce a stable current in the channel.

2.3 The width of the channel

One of the objectives in designing a channel is to decrease the wave-driven currents going out through the breakers, see Figure 2.2 black arrows. When no wave breaking occurs in the channel the cross-shore set-up in the channel is smaller than on both side parts of the reef. The incoming waves break over the submerged reef inducing a wave mass flux towards the shoreline; this flux then enters the area enclosed by the structure and the shoreline (see gray arrows in Figure 2.2). Moreover, the momentum associated with the incident waves creates a set-up of the mean water level over the reef resulting in a pressure gradient that subsequently pushes water into the same area. The convergence of these fluxes is expected to feed the currents leaving the rear of the

Figure 2.2 – Main wave and pressure induced circulation pattern over the ASR.

structure (black arrows in Figure 2.2): (1) one offshore current is expected to leave the sheltered area in the channel; (2) other offshore directed currents are expected to appear at both landward ends of the reef. The rip currents through the breakers are less intense than those in a design without a channel.

We hypothesize that by changing the width of the channel the overall circulation around the concerning reef can be controlled, or at least modified to create the desired circulation under different wave conditions. Varying the channel width was feasible because the right part of the reef (from wave makers) was designed to be moved across the basin.

Hydraulic behaviour of the physical scale model was studied by mean of measuring current velocities and water surface elevations. The set-up of the experimental study is detailed in the following chapter.

Experimental measurements were performed with the aim of getting insight into the hydrodynamic behaviour of the surf reef designed by VAN ETTINGER (2005). Moreover, impact of the channel width on the wave-driven circulations around the reef was investigated. The physical model was constructed at a scale of 1:15 in a wave basin which measures 30 m in length and 15 m in width; the water depth was 0.4 m. The three wave paddles, 15 m long in total, were programmed to generate regular and irregular waves. The reef was located on a 1:20 plane slope which functions as a beach. The smooth concrete bottom of the basin ensures minimal friction dissipation on the flat part between the wave makers and the plane slope. In the following, a description of the instruments used during the experiment is given. After that, the test conditions are described. Finally, detailed procedures of experiments are explained in section 3.3.

3.1 Instruments

Fluid motion in the basin was generally measured in two forms: water surface elevation and current velocity respectively. Measurements of water surface elevations, which were then translated into wave parameters, were recorded by using Resistance Wave Gauges (GHMs). The wave gauge consists of two parallel stainless steel rods. During measurement, wave gauges are placed at the measuring points while ensuring that the top of the plastic head (reference-electrode) is at least 4cm under the water surface and the wave crest meets both rods simultaneously. In some cases, several GHMs were placed close to each other however a minimum distance of 20cm was restricted to prevent any mutual influence. One wave gauge was always positioned 3m in front of the wave makers to measure the generated wave field. To determine how waves break on the reef, water surface elevation was measured at a number of points along both the left and the right part.

To measure the currents in the basin two techniques were employed. The first one uses Electromagnetic Flow Meters (EMS) to obtain velocities in x and y -direction, see Figure 3.1. With this kind of EMS, current can be measured up to a distance of 0.5cm from the bottom and side-walls.

The second method utilises digital imaging to analyse movements of floats, thereby providing information of the Lagrangian surface flow characteristics. The camera is a conventional Panasonic digital camera equipped with a fish eye lens to capture the below basin area. The camera resolution is 576x720 pixels and records with a frame rate of 25Hz. Table 3.1 summarises the measurement equipments.
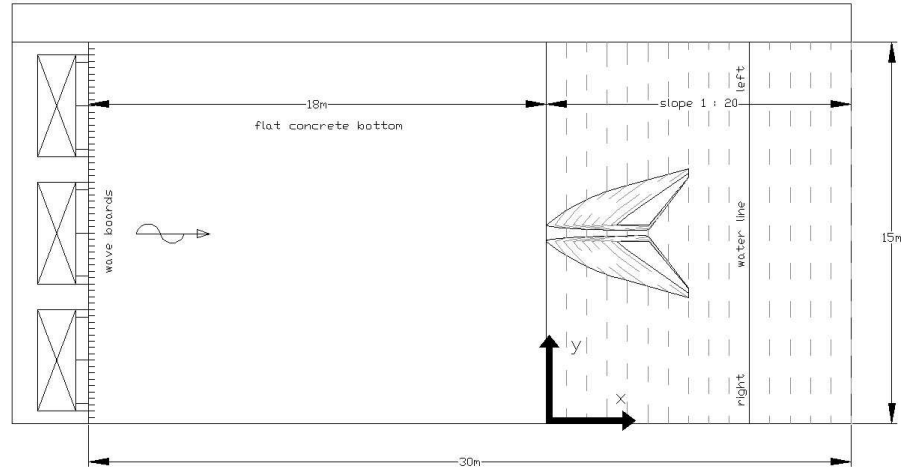
Figure 3.1 – Top view of the wave basin.

The GHM and EMS were mounted on either a wooden beam or a tripod which can be moved around the basin to cover the selected points. The EMSs were always measuring at one third of the water depth above the basin bed corresponding to the depth-averaged velocity in the case of a logarithmic vertical velocity distribution. The EMS requires a water depth of at least 10 cm to give a sufficient accurate measurement. A shoreward boundary was also applied for the float tracking techniques: the float movements were analysed as long as they were 2m away from the still water line.

Table 3.1 – Measurement equipments.

Measurement instrument	Number
Electromagnetic Flow Meter (EMS)	5
Resistance Wave Gauge (GHM)	5
Digital camera	1
White float	500

3.2 Test conditions

The measurements were performed under four different wave conditions: bi-chromatic wave B1, irregular wave I1, monochromatic wave M2, and monochromatic wave M1 respectively. Wave parameters of different conditions are tabulated in Table 3.2. The characteristics of B1, I1 and M2 were chosen to ensure that wave condition has equal wave energy to each other, for detailed calculations see Appendix A. The monochromatic wave M1 contains the most powerful energy compared to the rest. The bi-chromatic wave was originally obtained by scaling down the wave condition used for designing the existing ASR (VAN ETTINGER, 2005). In which the two component frequencies are 0.518 Hz and 0.448 Hz, respectively, and every seventh wave is the biggest wave with a wave height of up to 0.1m.

Table 3.2 - Wave conditions

Case	Wave type	H [m]	f [Hz]	U
B1	Bichromatic	0.1	$f_1 = 0.518$ $f_2 = 0.448$	23.1
I1	Irregular	$H_S = 0.1$	$f_P = 0.483$	23.1
M1	Monochromatic	0.1	0.484	23
M2	Monochromatic	0.07	0.483	16.3

The wave makers are not equipped with reflection wave compensation and can produce only unidirectional waves normal incident to the plane slope of the basin. Three wave boards are controlled to move simultaneously in phase and amplitude by a steering signal from a single computer. Delft-AUKE software is used to create the steering signal files taking into account the limitation of the wave makers.

A restriction to the bi-chromatic and monochromatic wave conditions results from the requirement that Stokes second-order wave theory should be valid at the given wave makers. A measure for the relative amplitude of the bound super harmonic is given by the Ursell number ($U = HL^2/h^3$). In which, h is the water depth, H is the wave height and L is the wavelength at the wave makers. Stokes second-order theory is no longer valid for Ursell number large than 25. Second-order wave board control was used to generate second-order Stokes waves and to minimise spurious second-order free wave generation (MADSEN, 1971).

With the exception of wave condition I1 (Jonswap energy spectrum) the second-order wave board control was not switched on due to the limitations of the wave makers.

3.3 Measurement procedure

GHM and EMS

The data of the wave gauges and flow meters was acquired at a sampling rate of 25Hz. The smallest wave frequency is around 0.483Hz, so the sampling rate is much larger than twice the wave frequency being sampled. To check the statistical stability of the experiment, every measurement was repeated two or three times.
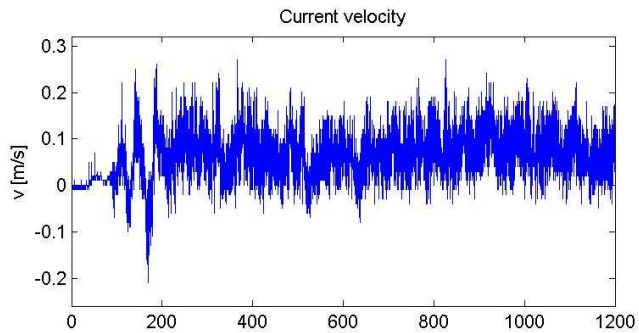
Figure 3.2 – Cross-shore current velocity variation at a certain point in the basin.

Some first measured tests with GHMs and EMSs were 30 minutes in order to estimate the necessary time for the current to develop in the basin. EMS data shows that the necessary duration for a quasi-stationary situation in the basin is approximately 10 minutes, see

Figure 3.2. For regular wave condition, measurement of some minutes seems sufficient, irregular waves, however, request a longer duration to achieve better spectral resolution (HUGHES, 1993): 10 minutes (300 waves) is supposed to be sufficient to obtain reliable spectra analysis for the Jonswap energy spectrum. All measurements with GHM and EMS were therefore recorded during 20 minutes; from the acquired data the last 10 minutes were then averaged to obtain the mean values.

PTV technique

To obtain the surface pattern of the wave-driven currents over the reef with Particle Tracking Velocimetry (PTV) technique, about 500 white floats were distributed into the wave basin and filmed from elevated positions. The float movements over the reef were captured in two parts: the left and the right (see Figure 3.3).

After around 10 minutes of running waves when the circulation gets stable, the camera is started and in approximate a couple of minutes about 200 floats have to be thrown into the desired filming area. In the next 10 minutes, floats are continuously distributed into the basin to ensure that a certain number of particles continue to appear in the filmed area. In this period, floats are placed outside the desired area in such places that floats are forced into the area by waves or currents. The image series of each recorded movie were processed by subtracting the undisturbed image, cropping the area of interest and transforming to gray scale. These gray scale images were then analysed with an advanced Particle Tracking Velocimetry program (VAN DER PLAS et al., 2003 and BASTIAANS et al., 2001). This yields information of position, velocity and pixel coordinates of the white floats during the measurements. Translating the results into the laboratory coordinate system and interpolating the results on a grid, the average surface velocity pattern is retrieved for each layout and wave condition.

Recording with white floats was implemented with all wave conditions except the monochromatic wave M1. Experimental results are presented in the next chapter.
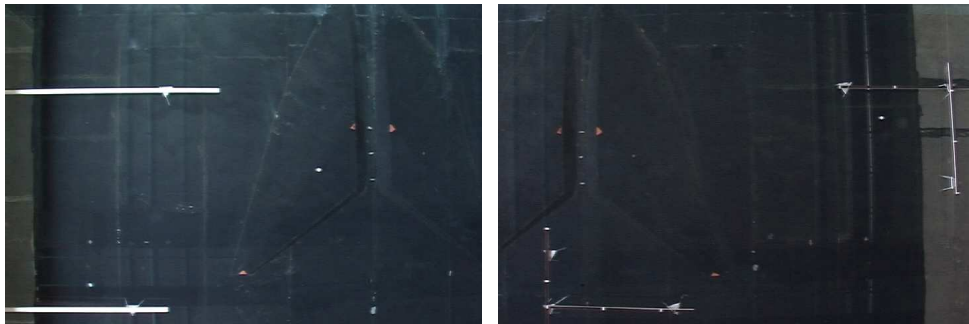
Figure 3.3 – Left filmed area (right panel) and right filmed area (left panel).

Three different reef layouts were tested to evaluate the influence of the width of the channel on the wave-induced flow circulation in the vicinity of the existing ASR. The width of the channel (W_{RC}) was the only dimension changed in the three layouts with the value of 0.64m, 1.2m and 1.8m. Wave conditions were the same for every layout. The measurement intensities were, however, not identical. Through this chapter, experimental results are separated into three main sections corresponding to three different layouts of the ASR. Each section generally presents data in three forms:

1. Wave height distributions (root mean square wave height) derived from water surface elevation recorded with GHM;

2. Surface circulation patterns obtained with PTV technique showing magnitude and direction of surface currents;

3. Velocity distributions attained with EMS representing current velocities at one third of the water depth from the bottom.

4.1 The first layout – $W_{RC} = 0.64$m

The width of the channel is defined as the distance in centimetre between two offshore head points of the left and the right flat crest of the reef. In this layout, $W_{RC} = 0.64$m. Positions of EMSs and GHMs in the wave basin are shown in Figure B.1, Appendix B. The corresponding mean values for the velocities and wave characteristics can be found in Table B.1, and B.2.

In the whole basin, water surface elevations were measured in 5 points. One wave height probe was always located 3m away from the wave makers measuring incident wave parameters. Four were symmetrically placed as shown in Figure 4.2: two at the beginning of the left and the right rides, where waves are going to break; two others on both sides the of plane slope, where water depth was sufficiently deep to prevent any wave from breaking.

Five EMSs were moved around the basin to cover 15 points, giving the depth-averaged velocity distribution plotted in Figure 4.1 (right panels), in which velocity vectors are proportional to the unit vector at the upper left corner. General, depth-averaged velocities are dominantly directed offshore except some small onshore directed vectors at the deep part of the channel ($x < 3$m and $h > 0.25$m).

As depicted in Figure 4.1 and 4.2, the wave height distributions and the mean circulation patterns are not symmetrical in contrast to the underlying reef layout.

Wave heights measured on the left side of the basin are bigger than on the right side; differences range between 5 and 10%. At the start of the wave rides, higher waves are also found on the left with variations of up to 5% for I1, M2 and M1. While B1 shows a significant asymmetry of wave height distribution on the reef, waves on the left are 13.5% higher than on the right.

As can be seen in Figure 4.1, the PTV-estimated surface velocity field shows a shoreward directed flux over the flat crests of the reef and in the middle of the rip channel. These velocities induced by breaking waves have maximum values of 0.12m/s for I1, 0.11m/s for B1 and 0.16m/s for M2. The maximum velocities of the outgoing rip-currents at either sides of the ASR are approximately 0.15/ 0.12, 0.18/ 0.13 and 0.18/ 0.19m/s (right/ left) for the respective I1, B1 and M2 wave condition.

The depth-averaged velocities measured with EMS instruments show seaward directed currents in nearly all the measuring points, except at several points in the rip channel representing minimal onshore velocities. The maximum velocities measured with EMSs are all located at both sides of the reef. Those are alternatively 0.225m/s for I1, 0.264m/s for B1 and 0.337m/s for M1 measured on the right flat crest where local water depth is 0.1cm, while for the M2 wave condition, the maximum value is 0.237m/s which is found at the left outgoing rip current.
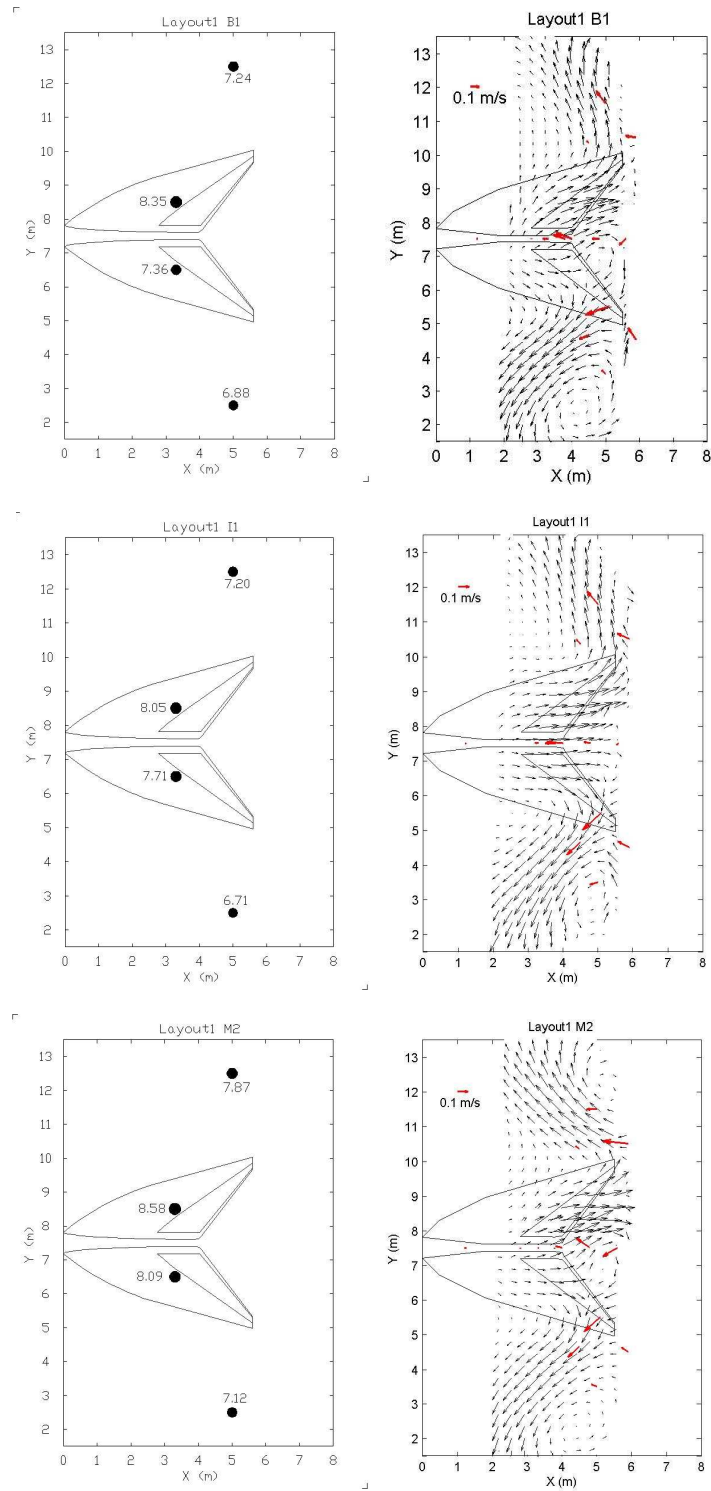
Figure 4.1 – First layout. Left panels: wave height distribution, in cm. Right panels: velocity distribution obtained with PTV technique (black arrows), EMS (red arrows). From top to bottom: bi-chromatic wave B1; irregular wave I1; regular wave M2.
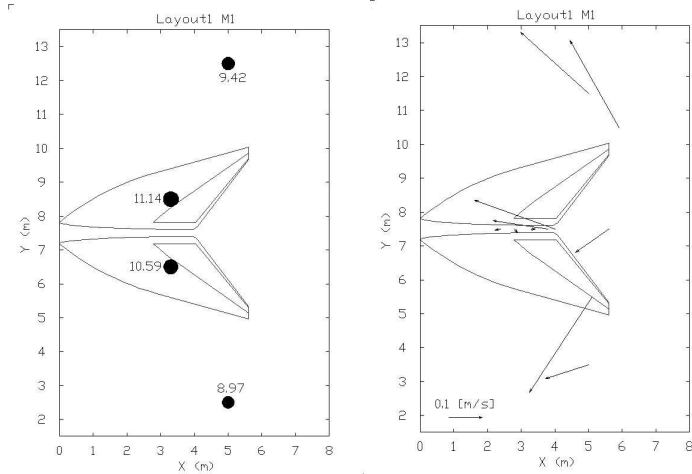
Figure 4.2 – First layout. Monochromatic wave M1. Left panel: wave height distribution, in cm. Right panel: velocity distribution obtained with EMSs.

The cross-shore velocity component obtained with EMSs along the channel axis is depicted in Figure 4.3, where negative value represents offshore flow. The maximum of all measured velocities (case B1, I1 and M1) appears at measurement point with $x = 4$m corresponding to the location of strong onshore surface velocity induced by breaking waves. For M2, the maximum is not achieved at this point and in contrast to other wave conditions the measured velocity increases when approaching the shoreline. The maximum seaward directed velocity in the narrowest channel is -0.142m/s for I1; -0.163m/s for B1; -0.139m/s for M2; and -0.239 for M1.
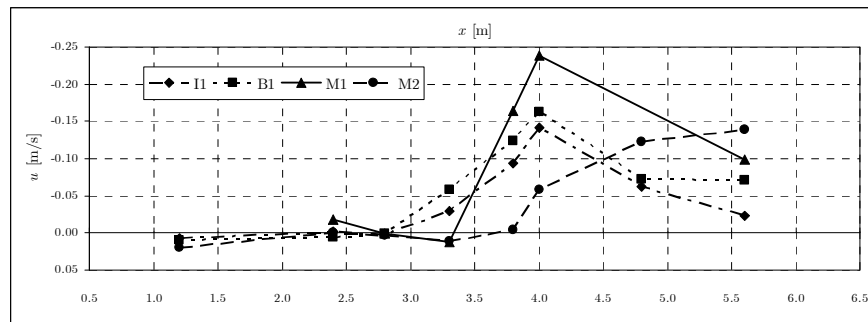
Figure 4.3 – First layout. Cross-shore velocity in the middle transect of the rip channel.

4.2 The second layout – $W_{RC} = 1.2$m

In the second layout, the right part of the reef was relocated further away from the left part resulting in a channel width of 1.2m that is expected to change the circulation fluxes and wave induced currents around the entire ASR. It is probable that a wider gap facilitates the offshore flow increasing the return flux through the channel. Consequently the amount of water leaving the rear of the structure in the rip currents through the breaker zones at either side of the ASR will be reduced. The reduction in current intensity of these rips then weakens the wave-current interaction resulting in longer surf rides.

The total number of points measured with EMSs in this layout is 15, similar to the first layout. In order to determine how waves break over the existing reef, GHMs were slid along either ride of the reef giving wave parameters at 6 points, see Figure 4.5 (left panels). Besides, water surface elevations were measured in the paddling channel and on both sides of the basin.

Similar to the first layout, there are still asymmetries in wave height and velocity distribution at the ASR in almost all wave conditions. Higher waves were measured on the left of the basin for B1 (6.2%), I1 (4.8%) and M2 (15.4%) wave conditions. Especially for monochromatic wave test M1, waves are symmetrically distributed on the plane slope across the basin. Figure 4.6 illustrates the alongshore wave height distributions at three x-coordinates and the corresponding bathymetries.
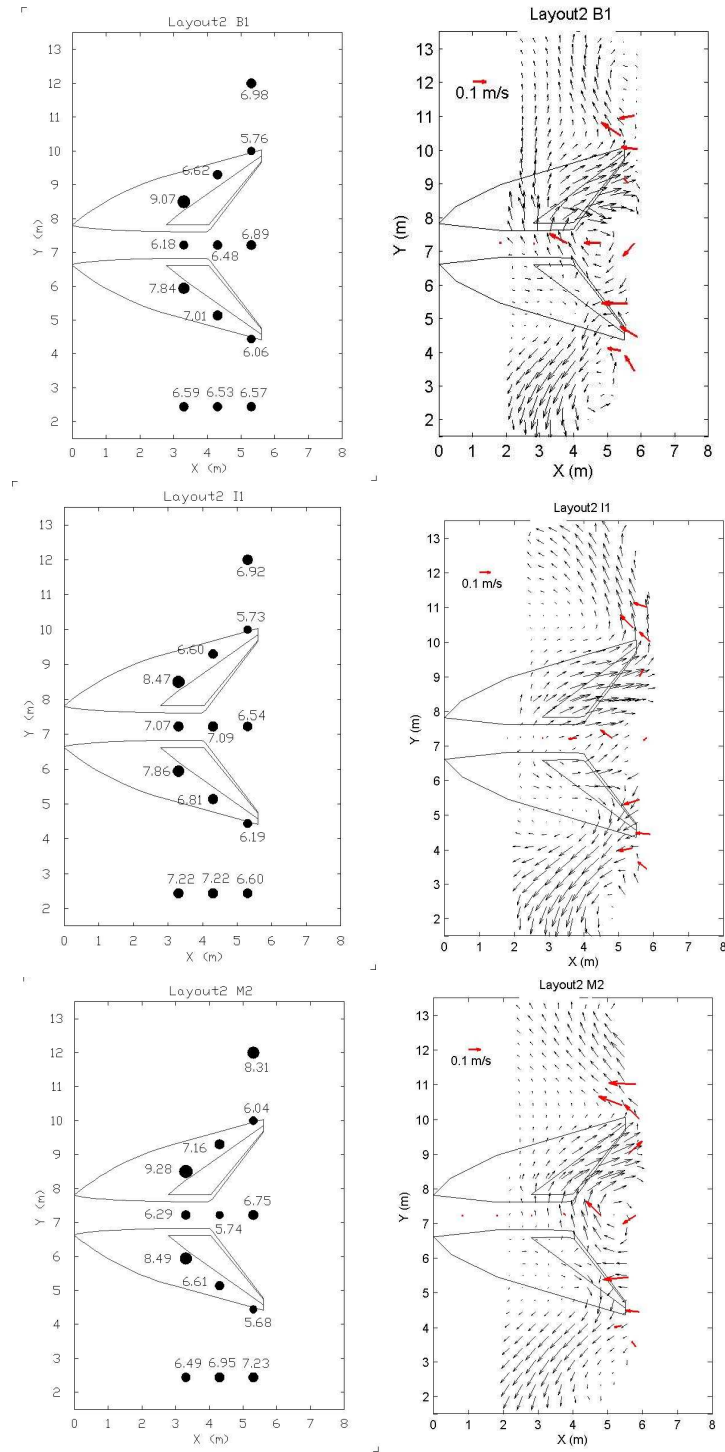
Figure 4.4 – Second layout. Left panels: wave height distribution, in cm. Right panels: velocity distribution obtained with PTV technique (black arrows), EMS (red arrows). From top to bottom: bi-chromatic wave B1; irregular wave I1; regular wave M2.
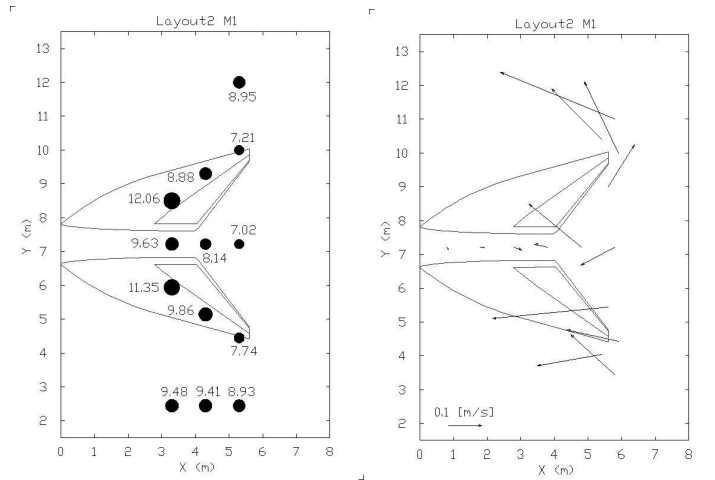
Figure 4.5 – Second layout. Monochromatic wave M1. Left panel: wave height distribution, in cm. Right panel: velocity distribution obtained with EMS.
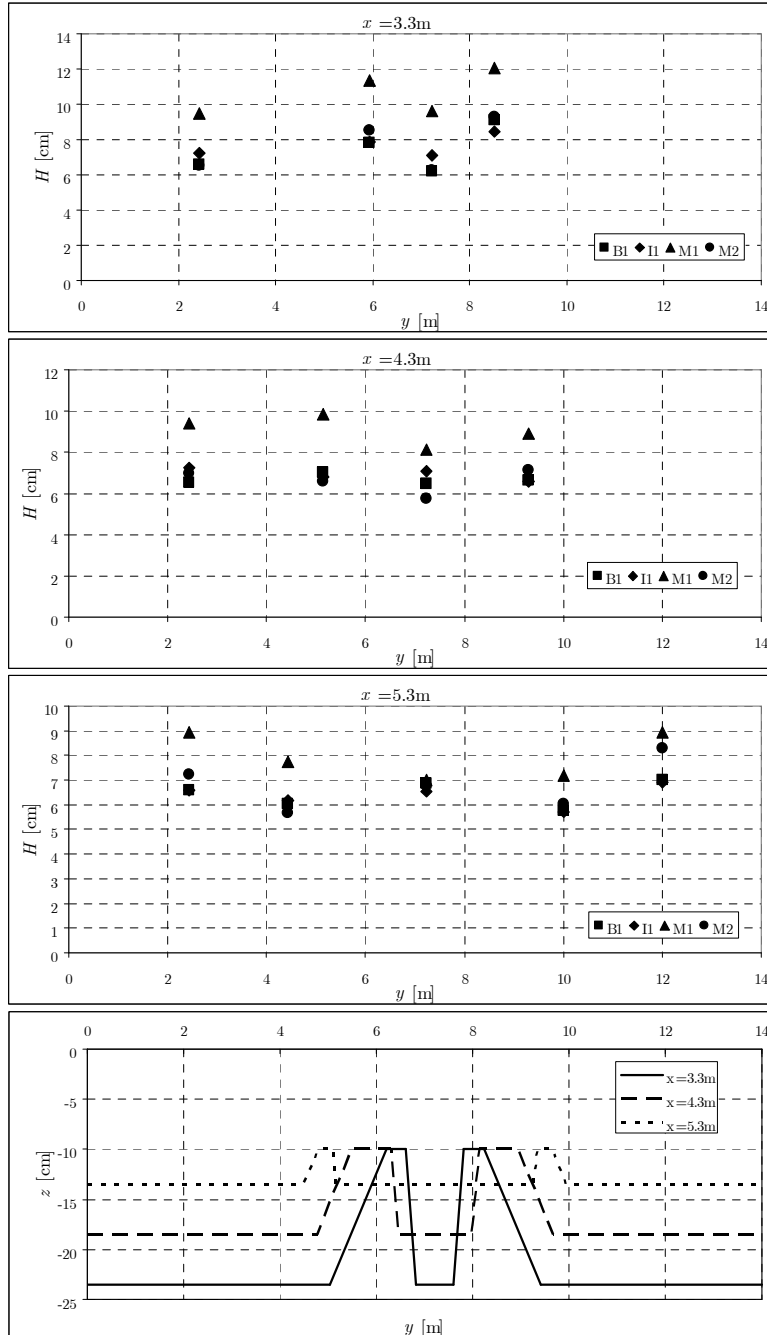
Figure 4.6 – Second layout. Alongshore (y-axis) wave height distribution. From top to bottom: wave heights measured at $x = 3.3$m; $x = 4.3$m; $x = 5.3$m; and alongshore bathymetry at different x-coordinates.

As can be seen in the PTV results (Figure 4.4, right panels, black arrows), there are two main differences with respect to the first layout. The first significant change is the absence in B1 and M2 and important decrease in I1 of the shoreward directed flux in the rip channel. Where previously there was an intense shoreward current, there is now an eddy circulation, in B1 and M2, or a really small shoreward directed flux of water, in I1. The second relevant feature that can be observed in the surface velocity circulation is the

weakening of the outgoing fluxes through the breakers. The maximum velocities measured in the second layout are around 0.13/ 0.12m/s, 0.16/ 0.11m/s and 0.14/ 0.16m/s, (right/ left) for I1, B1 and M2 wave condition, respectively.

Considering the mean circulation obtained with EMSs (Figure 4.4, right panels, red arrows; Figure 4.5, right panel), the maximum velocities are located at either sides of the reef. Within those, some are found on the left side of the reef: 0.155m/s for I1; 0.218m/s for M2 and 0.368m/s for M1, while a maximum value of 0.187m/s was recorded on the right for B1. All the results measured with EMSs during this second layout can be found in Table B.3, Appendix B.

The cross-shore current along the rip channel has maximum seaward directed velocities of -0.097m/s with I1, -0.124m/s with B1, -0.118m/s with M2 and -0.155m/s with M1 (Figure 4.7). These maximum values are found at a distance of 3.8m and 4.8m from the beginning of the slope for B1 and the rests, respectively.
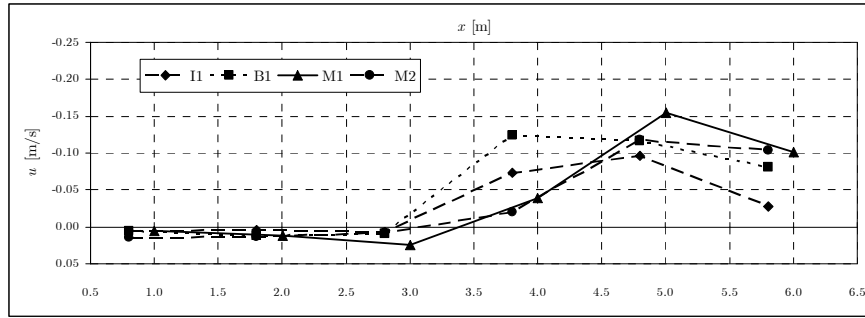
Figure 4.7 – Second layout. Cross-shore velocity in the middle transect of the rip channel.

4.3 The third layout – W_{RC} = 1.8m

It was expected that the last layout would provide the best surf-ability behaviour due to the more intensive weakening of the wave-induced interactions at both sides of the existing ASR. The third layout was therefore measured more extensively either in the rip channel or around the lateral sides of the reef. In Table B.5, B.6 Appendix B positions of instruments can be found together with average measured values.

The asymmetry in wave height distribution shows that higher waves are found on the left side. On the reef, variations of wave height show a complex pattern when higher waves are sometime found on the right wave ride. Figure 4.10 illustrates the alongshore wave height distributions at three x-coordinates and corresponding bathymetries.
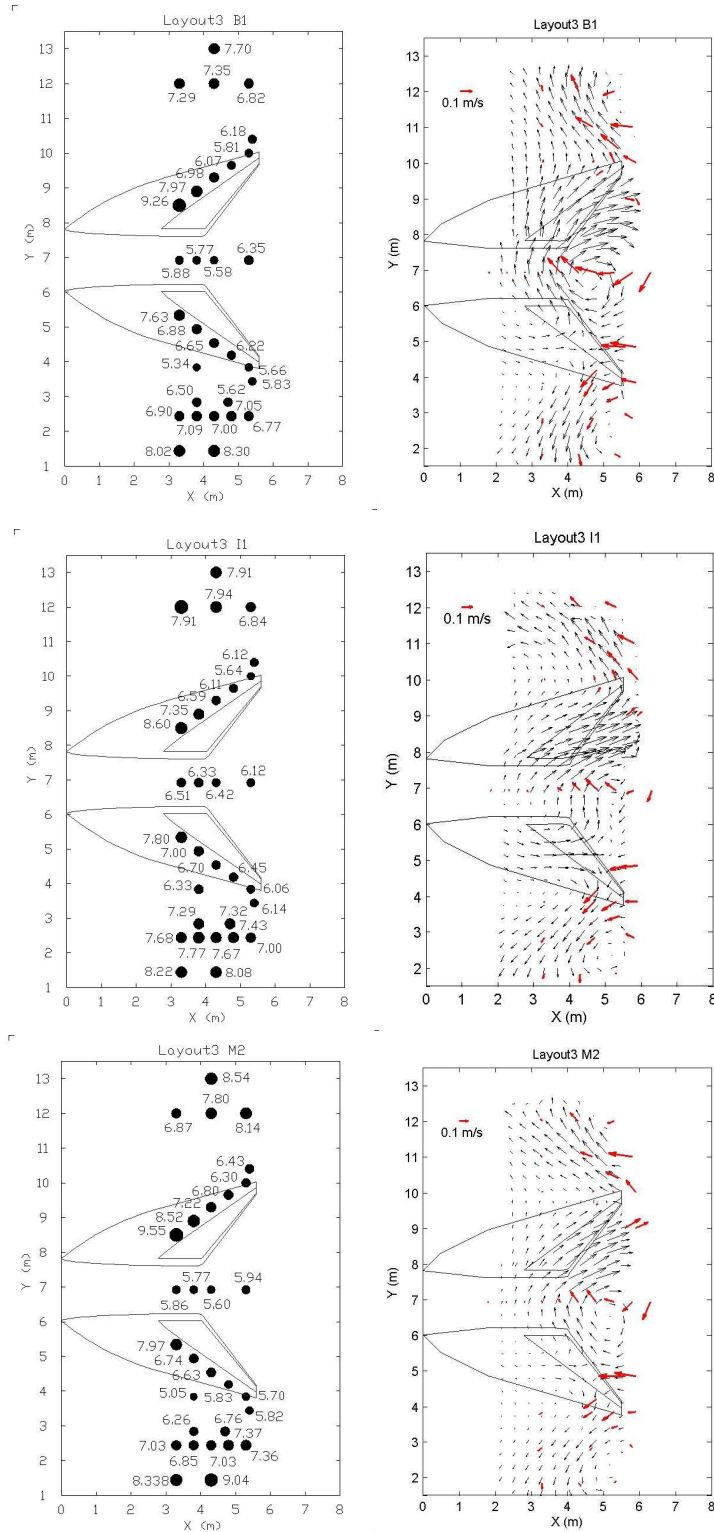
Figure 4.8 – Third layout. Left panels: wave height distribution. Right panels: velocity distribution obtained with PTV technique (black arrows), EMS (red arrows). From top to bottom: bi-chromatic wave B1; irregular wave I1; regular wave M2.
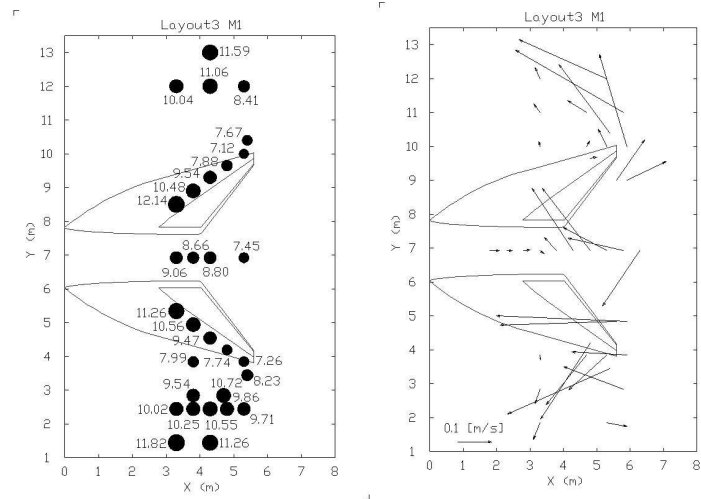
Figure 4.9 – Third layout. Monochromatic wave M1. Left panel: wave height distribution. Right panel: velocity distribution obtained with EMS.
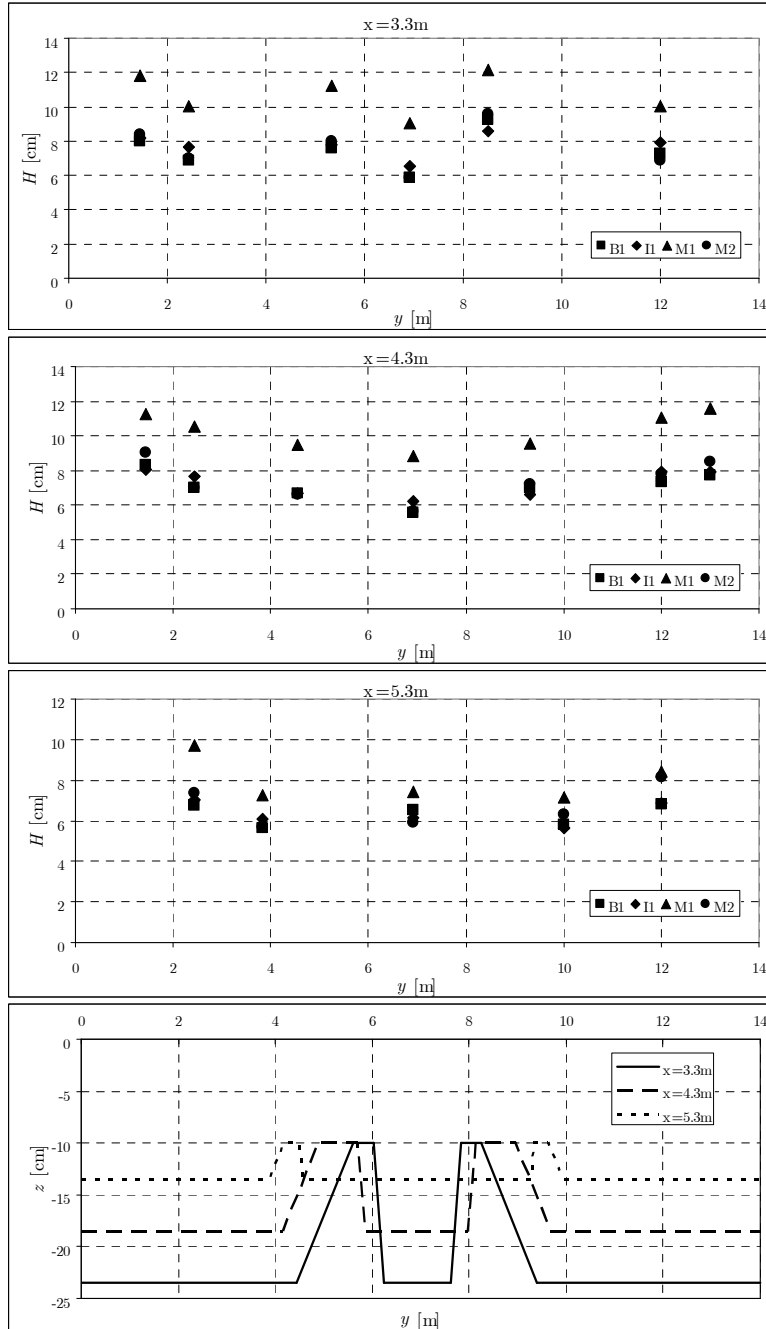
Figure 4.10 – Third layout. Alongshore (y-axis) wave height distribution. From top to bottom: wave heights measured at $x = 3.3$m; $x = 4.3$m; $x = 5.3$m; and alongshore bathymetry at different x-coordinates.

The PTV-estimated surface velocities obtained for this final layout show that there is indeed a reduction of the rip currents on both sides of the ASR. The maximum surface velocities measured are approximately 0.10/ 0.11m/s, 0.12/ 0.13m/s and 0.14/ 0.16m/s, (right/ left) for I1, B1 and M2 wave conditions, respectively. The previously observed eddy circulation at the rear of the ASF (B1 and M2 at the second layout in Figure 4.5) has now increased in dimension and intensity and seems to controls the circulation at the rear of the

24

structure. The eddy is also present during the irregular wave conditions, but less intense than for the monochromatic and bi-chromatic wave conditions.

The cross-shore velocities measured at 9 points along the rip channel axis with EMS show an intense offshore discharge at the rear of the structure, see Figure 4.11. Maximum measured cross-shore velocities at this transect are: -0.112m/s at $x = $ 4.8m for I1; -0.173m/s also at $x = $ 4.8m for B1; -0.109m/s at $x = $5.3m for M2; and -0.166m/s at $x = $ 5.8m for M1.
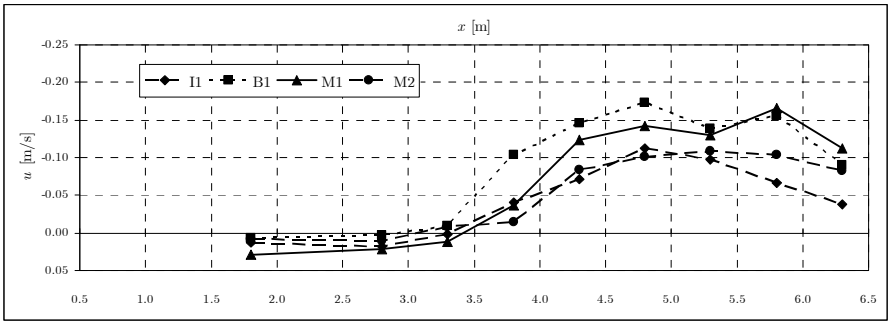
Figure 4.11 – Third layout. Cross-shore velocity in the middle transect of the rip channel.

5.1 Wave heights

Alongshore variations

On the plane slope, GHM positions were restricted to be out of the breaker zone, hence the measured waves are non-breaking waves. Moreover, these points are moreover located at certain distances from the structure to ensure that wave propagation is normal to the straight and parallel depth contours of the 1:20 slope. The existences of asymmetry in the wave height distribution were verified through all the measurements. In almost all tests, waves measured on the left side of the basin slope are higher than on the right side with differences mostly ranging between 4 and 10%, see Figure 4.6 and 4.10. Waves measured over the two reef parts also exhibit asymmetries, however, more complex since higher waves are found on either the left or the right.

The presence of the reef induces alongshore variations in wave height that dominantly control the circulation around the structure. In the present case of an asymmetry in alongshore wave height distribution, the higher waves would break further offshore at the left side of the reef, resulting in a stronger wave and pressure induced flux at the left side of the basin that exits through the breakers at the right side of the ASR. This effect is clearly observed in Figure 4.1 with a more intense circulation above the left part of the ASR (wave mass flux due to wave breaking) and a more intense rip current through the breakers on the right side of the basin.

The asymmetry in wave height distribution is likely due to errors in the wave generations. Besides, discrepancies in the underlying basin bathymetry can also cause asymmetry in the wave fields. By using levelling instruments, differences in bed level along the plane slope were recognised with a maximum deviation up to 10 mm for points at equal x positions. After the first layout, the right part of the reef was relocated on the plane slope of the basin. Before conducting measurements with the second layout, reef bathymetry was checked in order to explain the asymmetry in energy distribution. The basin was filled up with a certain discharge while a digital camera mounted above the reef was recording the increase of the water level. The entire movie was then transferred into separate images to analyse the geometrical shape of the reef. Differences in water lines surrounding the left and the right part of the reef were found but acceptable.

Figure 5.1 – Water rising up on the reef. From left to right: water depth is 10, 20 and 30cm.

Heterogeneous operation of wave makers and differences in the basin bathymetry are likely the main mechanisms inducing asymmetry in wave height distribution which results in another asymmetry in wave-driven circulation system around the existing ASR.

Cross-shore variations

Based on measured data from the second and the third layout, it is clear that cross-shore variations in wave height show quite different patterns under different wave conditions. For I1 and M1 wave heights decreased when propagating from water depth of 0.235 m ($x = 3.3$ m) to water depth of 0.135 m ($x = 5.3$ m) in the channel and also on both sides of the plane slope. In contrast, the monochromatic waves M2 perform increasing wave heights when propagating the same distance shoreward. Bi-chromatic waves B1 show mild variations in wave height on either side of the basin but an increase of up to about 10% along the channel in both layouts.

Table 5.1 – Cross-shore variations in wave height from water depth of 0.235 m (at $x = 3.3$ m) to water depth of 0.135 m (at $x = 5.3$ m). (-) presents a decrease in wave height and (+) for an increase.

Second layout

Wave case	Left	Rip channel	Right
I1		-7.5%	-8.3%
B1		+11.5%	0%
M2		+7.3%	+11.4%
M1		-27.0%	-5.8%

Third layout

I1	-13.5%	-6%	-8.9%
B1	-6%	+9.4%	-2%
M2	+16.5%	+1.4%	+4.7%
M1	-16.2%	-17.8%	-3.2%

The increase in wave height under M2 wave condition can be explained by shoaling theory when the wave propagation is assumed normal to the straight and parallel depth contours (Battjes, 1984). Shoaling coefficient ($K_S = H'/H_{S1}$) were calculated based on linear-

theory when waves are propagating on the plane slope of the basin and in the rip channel for M1 and M2 wave condition. H' is the calculated local wave height and H_{S1} is wave height measured at points S1, 3 m away from the wave makers. Besides, K_S values were calculated by normalising the measured wave heights by H_{S1}. Figure 5.2 shows that under M2 wave condition, measured data is relatively in accordance with results calculated based on linear-theory while an opposing pattern is found under M1.
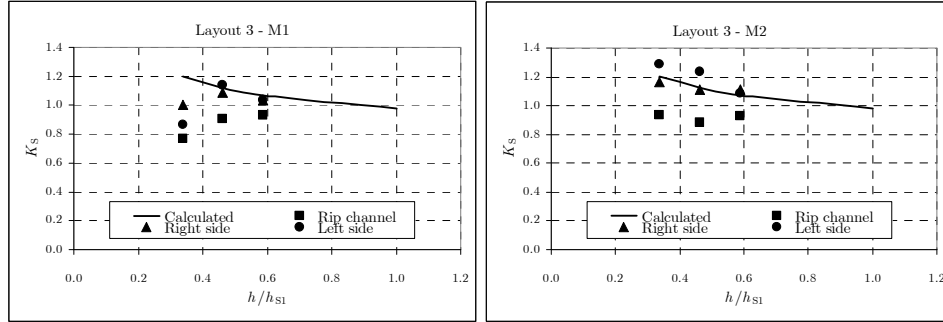
Figure 5.2 – Shoaling factor $K_S = H / H_{S1}$ versus h / h_{S1} for monochromatic wave M1 (left panel) and M2 (right panel). Symbols are measured data. Solid line is shoaling curve calculated by linear-theory.

In general, it is not consistent to explain the complex behaviour of wave heights under B1, I1 and M1 wave conditions as mentioned above with the linear theory of shoaling. The asymmetry in wave-induced circulation would induce impacts on the wave propagation, particularly variations in wave height. This prediction is recommended for further investigation.

Height reinforcement

Figure 5.3 illustrates the wave height distributions along the two parts of the reef. As three wave conditions B1, I1 and M2 were generated to have the same energy, wave heights of these wave conditions are comparable. Monochromatic waves M1 have larger wave heights compared to the other wave fields.

At the seaward tips of the two reef parts, waves are enhanced in height and start breaking. In the second and the third layout, when propagating along the reef waves are all decreased between 20 and 40% in height. Waves are always higher at the start of the left ride and the left ride also experiences more significant variation in wave height.
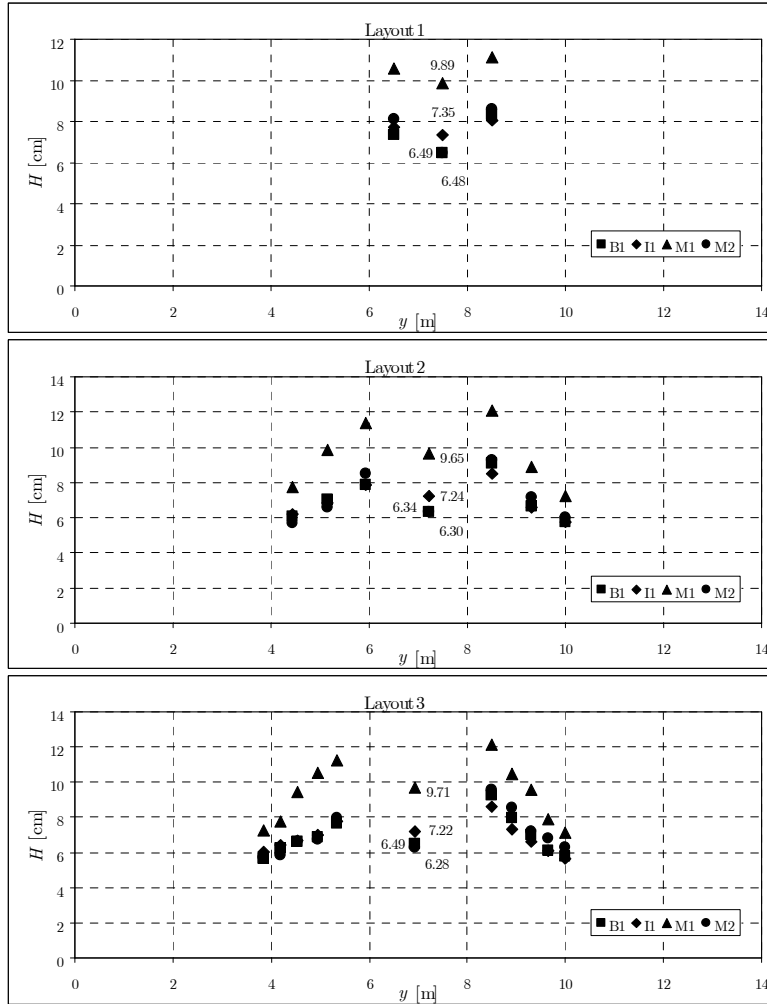
Figure 5.3 – Wave height distribution along the two reef parts projected on y-axis in the first layout (upper panel), the second layout (middle panel) and the third layout (lower panel). Marks attached with values are wave heights measured at S1, 3m away from wave boards.

The ratio of wave height measured on the reef to the wave height measured at point S1, 3m away from the wave boards, is defined as reinforcement factor ($K = H / H_{S1}$). Table 5.3 presents wave heights measured at S1; reinforcement factors at the start and the end of the rides; and the reduction in %, denoted as Δ, derived by comparing the reinforcement factors at the start and the end of the wave rides. In general, K values obtained at the start of either ride increase through the first to the third layout while opposite patterns are found at the end of both wave rides however with significantly smaller variations.

Table 5.2 – Wave height reinforcement.

First layout

Wave	H_{S1}	K on left ride [cm]			K on right ride [cm]		
case	[cm]	Start	End	Δ [%]	Start	End	Δ [%]
B1	6.84	1.22			1.08		
I1	7.35	1.09			1.05		
M1	9.89	1.13			1.07		
M2	6.48	1.32			1.25		

Second layout

B1	6.34	1.43	0.91	36.49	1.24	0.96	22.68
I1	7.24	1.17	0.79	32.33	1.09	0.86	21.20
M1	9.65	1.25	0.75	40.26	1.18	0.80	31.81
M2	6.30	1.47	0.96	34.92	1.35	0.90	33.03

Third layout

B1	6.49	1.43	0.89	37.29	1.18	0.87	25.77
I1	7.22	1.43	0.78	45.30	1.08	0.84	22.28
M1	9.71	1.25	0.73	41.34	1.16	0.75	35.56
M2	6.28	1.52	1.00	33.99	1.27	0.91	28.49

5.2 Currents

Surface circulations

The changes in the surface velocity patterns can be verified with the PTV measurements when the channel width is increased from 0.64 m to 1.2 m and finally 1.8 m. These changes are mainly found in: (1) direction and intensity of the velocities around the channel; (2) and in the rip current intensity through the breakers.

In the first layout, the surface velocities are directed shoreward in the channel, where an eddy circulation is found in the second and the third layout. Particularly under the bichromatic waves and the monochromatic waves, this eddy shows an increase in dimension and intensity as the channel gets wider. It seems to be the asymmetry in wave height distribution in the basin that controls the observed vortex. On the left side, higher waves break earlier and induce more vigorous wave mass fluxes than ones experienced on the right side. The existing differences between both sides of the basin may create the eddy circulation measured on the rear side of the reef.

At the start of the left part of the reef, waves are always higher than those of the right. However as can be seen in Figure 5.3, higher waves can be found along either the right part

or the left part. As a mutual interaction, the eddy possibly has impact on the variations of wave height along the reef and also the previously mentioned complex behaviours of propagating waves.
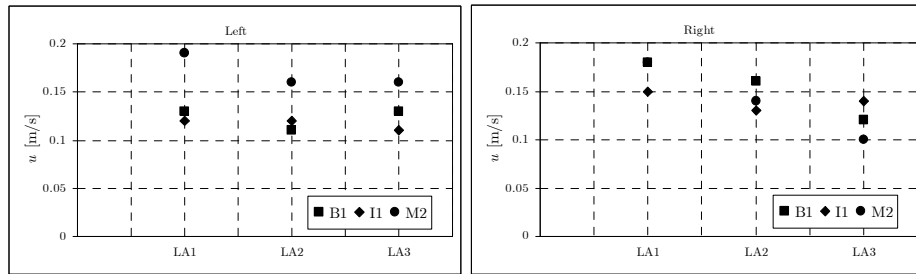
Figure 5.4 – Average surface velocities on the left side of the reef (left panel) and on the right side (right panel). LA1, LA2 and LA3 refer to the first, the second and the third layout.

Figure 5.4 shows that velocities (obtained with PTV technique) in the rip currents at both sides of the structure exhibit considerable reductions when widening the channel width. The changes in the averaged surface velocities on the left are less significant than those experienced on the right.

In summary, the eddy circulation is induced and governed by an asymmetry in wave height distribution on either side of the basin. The general basin surface circulation is certainly influenced by the presence of this eddy. With a clockwise direction and dominant intensity over the left part of the reef the eddy circulation is believed to nourish the left side rip current consequently preventing a large decrease of its intensity.

Depth-averaged flow velocities

The changes in the depth-averaged flow velocities due to the widening of the channel are more problematic to quantify because of the differences in the numbers of measured points as well as their positions in the basin coordinate. On either side of the reef, currents are generally directed offshore to go out through the breakers. Measured velocities in the channel exhibit a smooth decrease with an increase in the width of the channel. Currents in the channel are dominantly directed offshore except at some points in the deep part, however, with very small intensities. The maximum offshore directed velocities measured along the channel axis in three layouts are plotted in Figure 5.5.
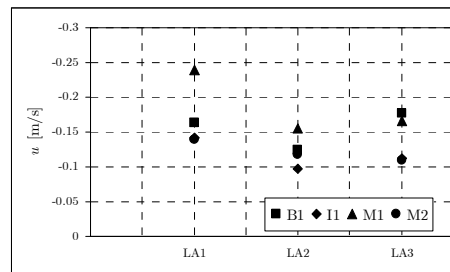
Figure 5.5 – Maximum offshore directed velocities measured along the channel axis. LA1, LA2 and LA3 denote the first, the second and the third layout respectively.

5.3 Wave-current interactions

Despite the decrease in wave height along either wave rides of the reef, observations during the three layouts show that waves were generally breaking in the plunging regime on either part of the reef except a short part at the end of the right part. Breaking shapes of monochromatic wave M2 were captured along both parts of the reef as depicted in Figure 5.8. At the end of the right wave ride (point S6 and S26), waves were breaking in a spilling manner. This is due to the fact that the rip currents on the right side of the reef were always more significant than on the left, which are obviously depicted in Figure 4.1, 4.4 and 4.8. Wave-current interaction plays an important role in this area inducing negative impact on the breaking shapes. When wave experiences an opposing current, wave length is decreased and wave

Figure 5.6 – Third layout. GHMs are located along wave rides.

steepness is consequently increased. Relating to Iribarren number $\xi_b = \tan\alpha / \sqrt{H/L}$ (BATTJES, 1974), it is clear that decreasing local wave lengths lead to decreasing ξ_b values, hence waves break spilling.

Wave numbers were calculated with and without the presence of rip currents at 4 points on the reef (point S6, S7, S24 and S26 Figure 5.6) and the corresponding variations of wave steepness induced by these rip currents. Wave steepness is defined as $s = H/L$ with H and L is local wave height and wave length obtained with GHM and EMS. The method of calculation is explained in Appendix C, calculation results are presented in Table 5.3. Rip currents are opposing the incident wave direction at almost all measured points except point S24. Rip currents can be represented by Froude number $Fr = U_{rip} / \sqrt{gh}$, in which, $U_{rip} = \sqrt{u^2 + v^2}$ is the sum vector of two velocities components in x and y - direction measured with EMS, that will be used to determine the importance of wave-current interaction. On the left, rip currents with Froude numbers smaller than 0.1 gently decrease (less than 6%) or increase (less than 12%) the wave steepness, while those on the right with Froude numbers of 0.1 or much higher (up to 0.24) cause negative impact on the breaking shape of coming waves by significantly enhancing the wave steepness, mostly about 20%. Rip currents at the end of the left wave ride are low energy rip currents with $Fr < 0.1$ and those on the right are found to fall within the class of intermediate energy rip currents that have moderate wave-current interaction (MACMAHAN et al., 2006).

Table 5.3 – Variation of wave steepness with the presence of rip currents above the wave rides in the third layout. Opposing currents have negative sign (-u).

Bi-chromatic wave B1

Side	Left		Right	
Point	S24	S7	S26	S6
k	5.06	5.42	4.54	4.74
u [m/s]	0.06	-0.09	-0.19	-0.11
Froude	0.05	0.08	0.16	0.10
k'	4.74	5.99	5.65	5.37
Δs [%]	-5.95	11.57	25.62	14.29

Irregular wave I1

	S24	S7	S26	S6
k	4.76	5.09	4.56	4.76
u [m/s]	0.04	-0.09	-0.18	-0.16
Froude	0.04	0.08	0.16	0.14
k'	4.58	5.67	5.70	5.76
Δs [%]	-4.50	10.35	23.89	20.03

Monochromatic wave M1

	S24	S7	S26	S6
k	6.34	6.82	5.80	5.80
u [m/s]	0.02	-0.06	-0.27	-0.15
Froude	0.02	0.05	0.24	0.14
k'	6.17	7.37	8.11	7.10
Δs [%]	-2.07	7.54	48.59	22.12

Monochromatic wave M2

	S24	S7	S26	S6
k	5.32	5.73	5.04	5.04
u [m/s]	0.02	-0.02	-0.17	-0.16
Froude	0.02	0.02	0.15	0.15
k'	5.22	5.88	5.80	6.18
Δs [%]	-1.85	2.55	23.56	22.67

Figure 5.7 – Strength of rip current measured by Froude number, $Fr = u/\sqrt{gh}$ versus variation of wave steepness $\Delta s = s' - s$, where s' and s are wave steepness calculated with and without the presence of a rip current. Bold dashed vertical line divides the data into low and intermediate energy rip current regimes (MACMAHAN et al., 2006).

S3
S2
S27
S25
S5
S4
S24
S26
S7
S6
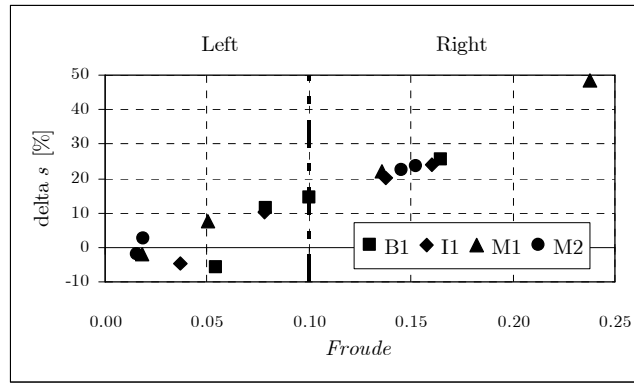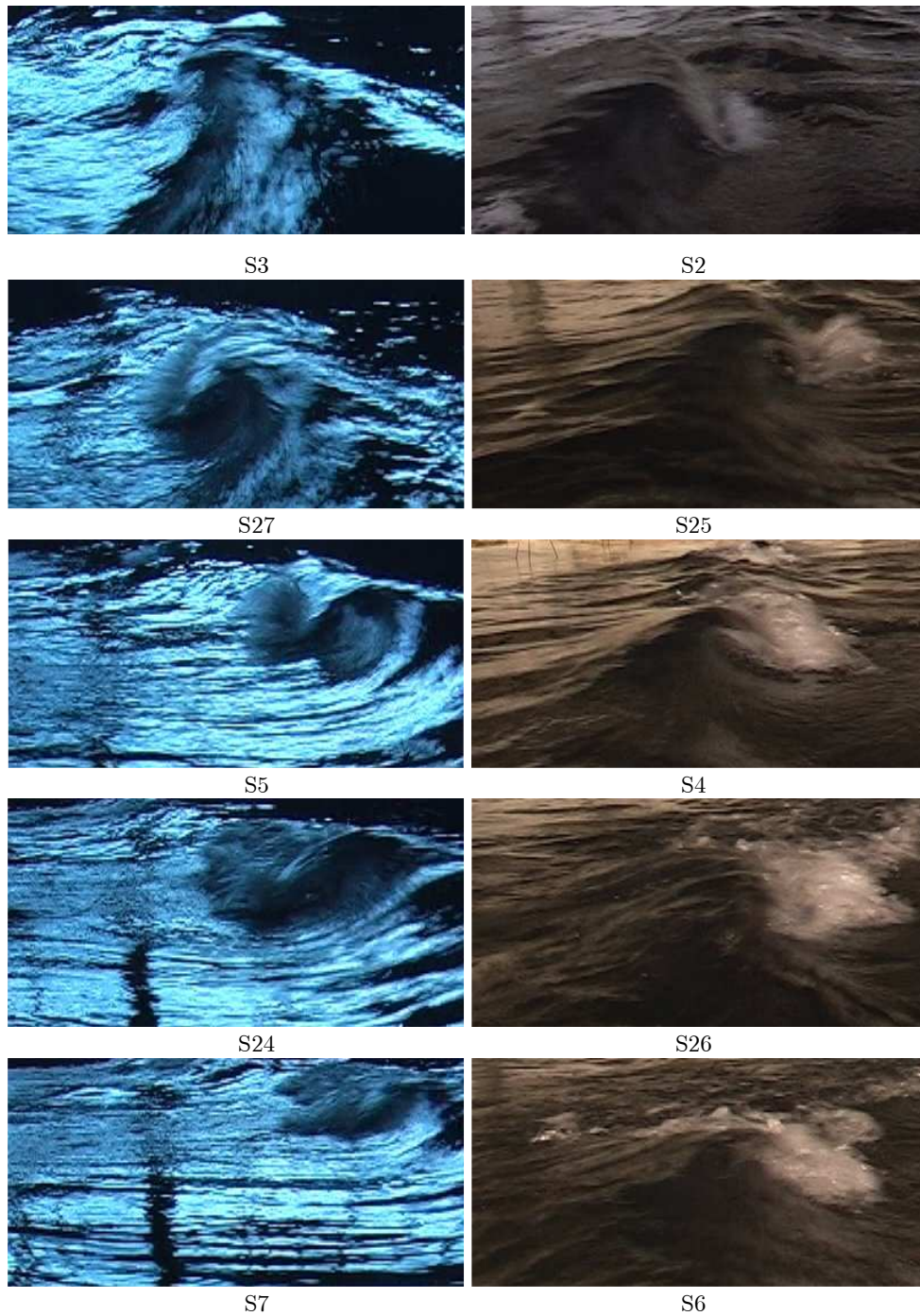
Figure 5.8 – Breaking shapes of monochromatic wave M2 along the left part (left panel) and the right part of the reef (right panel).

Conclusions and recommendations

6.1 Conclusions

An Artificial Surf Reef was designed with the purpose of improving the surf conditions, specifically for Dutch swell conditions (VAN ETTINGER, 2005). To optimise the reef design, proper understanding of wave-induced currents around an artificial reef is important for the performance with respect to surfing. Experimental measurements were performed in the present study to verify the impact of the channel width on the wave-induced circulations and the wave-current interactions around the concerning reef. Three kinds of data have been analysed: the depth-averaged velocities obtained with flow meters; the surface circulation velocities obtained by the use of Particle Tracking Velocimetry technique and the wave heights attained with wave gauges.

The depth-averaged velocities have been analysed mainly at both sides of the structure and in the middle of the channel. Through three different layouts, currents on either side of the reef show similar patterns, in which offshore direction is dominant spreading rip currents out of the surf zone. However, current intensities do not expose any significant variation. Measurements in the channel show a decrease in the maximum measured offshore velocities while increasing the width of the channel.

Considering the surface velocities two different phenomena can be found. Firstly, a decrease in velocities of the rip currents going above either side of the structure was recognised. Second observed phenomenon refers to the eddy circulation in the rear side of the structure. The eddy, which was induced by the asymmetry in wave height distribution along the basin, increases in either dimension or intensity with the widening of the channel. It is expected that in absence of the mentioned asymmetry, the eddy will never develop.

Wave heights were distributed asymmetrically and showed several complex variations in the entire wave basin. However, the reef generally performed well where waves were dominantly breaking in the plunging regime on either part of the reef. The reinforcement factors ranging between 1.08 and 1.52 were measured at the take-off of the final layout.

Low energy rip currents with Froude number smaller than 0.1 induce moderate impacts on surf-ability of the reef while more energetic rip currents (Fr >0.1) negatively affect the reef performance, particularly the desired plunging waves are eliminated due to wave steepening.

In summary, widening the channel decreases the surface wave-induced circulations in either intensity or dimension. The wave-current interactions at both sides of the reef are consequently reduced.

6.2 Recommendations

Water elevation variations according to tide conditions can affect the circulation around the reef and consequently the surf-ability. The impact of changing the water level on the performance of the existing reef is important to take into account.

Besides improving surfing conditions, ASRs are also designed and constructed for the purpose of coastal protection. The sediment transport processes around these structures are essential to investigate. Due to the capability of the existing instruments the velocity field close to the shoreline was not measured in this study, depth-averaged flow velocities were measured at least 2m away from the shoreline. The velocity distributions in this area have relevant importance when considering the accretion/ erosion sediment patterns that the proposed ASR will induce in the lee of the structure. In future work it will be desirable to extend the measurements towards this area in order to understand the effect of the channel width on the circulation pattern behind the reef. To do so, studying the behaviour of the existing reef in a moveable-bed basin can be of interest.

The existing reef was constructed such that it was smooth and impermeable, resulting in a small friction coefficient. To optimise the reef design, it is necessary to carry out simulation with more proper materials which would be expected to influence either the wave-induced currents or the surf-ability of the ASR.

The erroneous operations of the given wave makers obviously distorted the experimental results. These wave makers need to be closely tested in detailed and then corrected to perform properly. However, it could be interesting to simulate this kind of asymmetry in a numerical model to verify the phenomenon observed in the basin like eddy circulation.

ξ_b	Iribarren number, $\xi_b = \tan\alpha / \sqrt{H/L}$	[-]
E	wave energy	[J/m^2]
f	wave frequency $f = 1/T$	[Hz]
f_P	peak wave frequency of irregular wave	[Hz]
Fr	Froude number $Fr = u / \sqrt{gh}$	[-]
α	front slope angle experienced by normal incoming wave	[deg]
h	water depth	[m]
H	wave height	[m]
L_0	wave length in deepwater, $L_0 = gT^2 / 2\pi$	[m]
g	gravity acceleration	[m/s^2]
T	wave period	[s]
α_P	peel angle	[deg]
H_b	wave height along wave ride	[m]
H_0	the offshore wave height	[m]
N_L	the length scale ratio	[-]
W_{RC}	width of the paddling channel	[m]
U	Ursell number $U = HL^2 / h^3$	[-]
ρ	mass density of water	[kg/m^3]

BASTIAANS, R.J.M., VAN DER PLAS, G.A.J. and KIEFT, R.N., 2001. *The performance of high resolution particle velocimetry: algorithm, simulations and experiments.* Technical report, Eindhoven University of Technology. Report TUE-W, 2001-W-001, ISBN 90-386-2792-0.

BATTJES, J.A. 1984. *Short waves.* Lecture notes prepared for the International Institute for Hydraulic and Environmental Engineering, Delft.

BATTJES, J.A., 1974. *Surf Similarity.* Proc. 14th International Conference on Coastal Engineering, ASCE, Copenhagen, Denmark, pp 466 – 479.

BLACK, K.P. and MEAD, S., 2001. *Design of the Gold Coast Reef for Surfing, Public Amenity and Coastal Protection: Surfing Aspects.* Journal of Coastal Research, Special Issue No. 29, pp 115 - 130.

ETTINGER, H. D.V., 2005. *Artificial surf reef design.* MSc thesis, Faculty of Civil Engineering and Geosciences, Delft University of Technology.

HUGHES, S.A., 1993. *Physical Model and Laboratory Techniques in Coastal Engineering.* Advanced Series on Ocean Engineering – Volume 7, World Scientific, pp 97.

HUTT, J.A., BLACK, K.P. and MEAD, S.T., 2001. *Classification of Surf Breaks in Relation to Surfing Skill.* Journal of Coastal Research, Special Issue No. 29, pp 66 – 81.

MACMAHAN, J.H., THORNTON, E.B. and RENIERS, A.J.H.M., 2006. *Rip current review.* Coastal Engineering 53, pp 191 – 208.

HENRIQUEZ, M., 2004. *Artificial Surf Reefs.* MSc thesis, Faculty of Civil Engineering and Geosciences, Delft University of Technology.

OVER, R.W.J., 2006. *Surf-ability of an ASR in irregular waves.* MSc thesis, Faculty of Civil Engineering and Geosciences, Delft University of Technology.

PATTIARATCHI, C., 2003. *Performance of an Artificial Surfing Reef: Cable Station, Western Australia.* Copedec VI, 2003, Colombe, Sri Lanka.

SYMONDS, G. and BLACK, K.P., 2001. *Predicting Wave-Driven Currents on Surfing Reefs.* Journal of Coastal Research, Special Issue No. 29, pp 102 – 114.

TURNER, I.L., LEYDEN, V.M., COX, R.J., JACKSON, L.A. and MCGRATH, J.E., 2001. *Physical Model Study of the Gold Coast Artificial Reef.* Journal of Coastal Research, Special Issue No. 29, pp 131 – 146.

VAN DER PLAS, G.A.J., ZOETEWEIJ, M.L., BASTIAANS, R.J.M., KIEFT, R.N. and RINDT, C.C.M., 2003. *RIV, PTV and HPV User's Guide 1.1.* Technical report, Eindhoven University of Technology.

WILLIAMS, J.M., 1985. *Tables of Progressive Gravity Waves.* Boston: Pitman Advanced Pub. Program.

DELFT HYDRAULICS LABORATORY, INSTRUMENTATION DEPARTMENT. *Manual for Wave – Height Meter (G.H.M.).*

DELFT HYDRAULICS LABORATORY, 1990. *User's Manual for the Delft Hydraulics Four Quadrant Electromagnetic Liquid Velocity Meter.*

http://en.wikipedia.org/wiki/Surfing

http://en.wikipedia.org/wiki/History_of_surfing

http://www.goldcoast.qld.gov.au/image_content/artificial_reef.jpg

http://www.deh.gov.au/discussion-groups/coastnet/msg00007.html

Parameters of the wave conditions M2 and I1 are chosen to ensure that they contain identical wave energy with bi-chromatic wave condition B1. Because wave energy is independent of wave frequency, the mean frequency of B1 is applied for M2 (mean frequency) and I1 (peak frequency f_P).

- **Bi-chromatic waves B1**

Bi-chromatic wave B1 consists of two wave components with similar wave amplitude ($a_B = 0.025$ cm). The wave energy is:

$$E = \frac{1}{2}\rho g a_B^2 + \frac{1}{2}\rho g a_B^2 = \rho g a_B^2 \qquad (A.1)$$

In which, ρ is the mass density of water and g is the gravity acceleration.

- **Monochromatic waves M2**

$$E = \frac{1}{2}\rho g a_M^2 \qquad (A.2)$$

Where a_M is the wave amplitude of M2.

- **Irregular waves I1**

$$E = \frac{1}{8}\rho g H_{rms}^2 \qquad (A.3)$$

$H_{rms} = \sqrt{8m_0}$ is the root mean square wave height of I1, $H_S = 4\sqrt{m_0}$ is the significant wave height with m_0 is the 0th order moment.

Calculation based on the above equations results in wave heights tabulated as follows:

Table A.1 – Wave conditions

Case	Wave type	H [m]	f [Hz]
B1	Bichromatic	0.1	$f_1 = 0.518$ $f_2 = 0.448$
I1	Irregular	$H_S = 0.1$	$f_P = 0.483$
M2	Monochromatic	0.07	0.483

Table B.1 – LA1_W$_{RC}$_64 - EMS positions and current velocities.

Point	x [m]	y [m]	h [cm]	Velocity u / v [m/s]			
				I1	B1	M1	M2
V1	2.40	7.50	28.00	-0.002	0.005	-0.018	0.000
				0.002	0.000	-0.004	0.002
V2	2.80	7.50	26.00	0.002	0.001	0.009	0.003
				0.002	-0.007	-0.011	-0.008
V3	3.30	7.50	23.50	-0.030	-0.058	0.012	0.011
				0.002	0.000	-0.001	-0.001
V4	3.80	7.50	21.00	-0.094	-0.124	-0.164	-0.005
				-0.001	0.043	0.025	-0.007
V5	4.00	7.50	20.00	-0.142	-0.163	-0.239	-0.058
				0.012	0.063	0.085	0.015
V6	4.80	7.50	16.00	-0.062	-0.073	0.000	-0.123
				0.010	0.001	0.000	0.085
V7	5.60	7.50	12.00	-0.023	-0.071	-0.099	-0.139
				-0.016	-0.064	-0.069	-0.078
V8	5.00	11.50	15.00	-0.096	-0.100	-0.202	-0.097
				0.115	0.135	0.180	-0.004
V9	5.90	10.50	10.50	-0.108	-0.111	-0.146	-0.235
				0.048	0.015	0.256	0.025
V10	4.50	10.35	17.50	-0.034	-0.020	0.000	-0.037
				0.040	0.013	0.000	0.025
V11	5.10	5.50	10.00	-0.165	-0.249	-0.186	-0.148
				-0.152	-0.088	-0.282	-0.133
V12	5.90	4.50	10.50	-0.103	-0.085	0.000	-0.062
				0.054	0.131	0.000	0.040
V13	5.00	3.50	15.00	-0.070	-0.041	-0.128	-0.051
				-0.021	0.038	-0.042	0.020
V14	1.20	7.50	34.00	0.007	0.009		0.020
				-0.005	-0.003		-0.001
V15	4.50	4.65	17.50	-0.119	-0.105		-0.107
				-0.110	-0.044		-0.099

Table B.2 – LA1_W$_{RC}$_64 - GHM positions and wave parameters.

Point	x [m]	y [m]	h [cm]	f [Hz] / H [cm]			
				B1	I1	M1	M2
S1	-9.75	7.50	40.0	0.50	0.64	0.51	0.50
				6.84	7.35	9.89	6.48
S2	3.30	8.50	13.0	0.68	0.74	0.81	0.72
				8.35	8.05	11.14	8.58
S3	3.30	6.50	13.0	0.65	0.73	0.82	0.69
				7.36	7.71	10.59	8.09
S4	5.00	2.50	15.0	0.76	0.79	0.82	0.74
				6.88	6.71	8.97	7.12
S5	5.00	12.50	15.0	0.82	0.79	0.90	0.82
				7.24	7.20	9.42	7.87
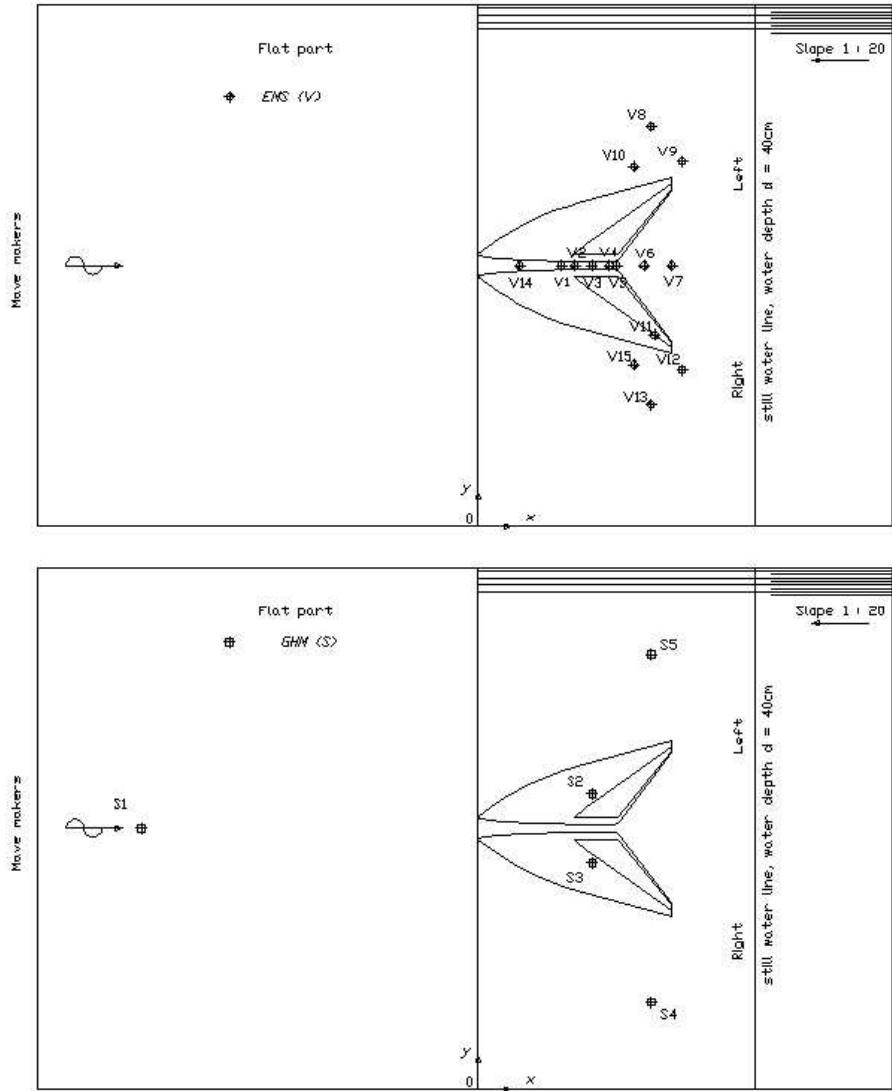
Figure B.1 – First layout. Measurement configuration: EMS (upper panel) and GHM (lower panel).

Table B.3 – LA2_W$_{RC}$_120 - EMS positions and current velocities.

Point	x [m]	y [m]	h [cm]	Velocity u / v [m/s]			
				I1	B1	M1	M2
V1	0.80	7.22	36.0	0.005	0.006	0.006	0.015
				-0.002	-0.003	-0.008	-0.004
V2	1.80	7.22	31.0	0.005	0.012	0.012	0.014
				0.000	0.003	-0.002	0.000
V3	2.80	7.22	26.0	0.007	0.009	0.024	0.008
				-0.001	-0.004	-0.009	0.000
V4	3.80	7.22	21.0	-0.074	-0.124	-0.039	-0.020
				-0.009	0.067	0.009	0.016
V5	4.80	7.22	16.0	-0.097	-0.116	-0.155	-0.118
				0.068	0.003	0.127	0.114
V6	5.80	7.22	11.0	-0.027	-0.081	-0.101	-0.104
				-0.020	-0.092	-0.054	-0.067
V8	5.40	4.04	13.0	-0.123	-0.098	-0.191	-0.059
				-0.026	0.017	-0.033	-0.011
V9	5.40	10.40	13.0	-0.107	-0.141	-0.148	-0.190
				0.113	0.095	0.150	0.071
V10	5.60	5.44	12.0	-0.142	-0.187	-0.344	-0.205
				-0.045	0.001	-0.034	-0.020
V11	5.60	9.00	12.0	0.031	-0.026	0.078	0.109
				0.059	0.037	0.124	0.101
V12	5.80	3.44	11.0	-0.078	-0.065	-0.132	-0.031
				0.062	0.110	0.119	0.043
V13	5.80	11.00	11.0	-0.114	-0.107	-0.340	-0.218
				0.036	-0.020	0.139	0.011
V14	5.90	4.44	10.5	-0.128	-0.127	-0.153	-0.107
				0.011	0.077	0.033	0.011
V15	5.90	10.00	10.5	-0.094	-0.118	-0.101	-0.119
				0.085	0.016	0.210	0.118

Table B.4 – LA2_W$_{RC}$_120 - GHM positions and wave parameters.

Point	x [m]	y [m]	h [cm]	f [Hz] / H [cm]			
				B1	I1	M1	M2
S1	-9.75	7.50	40.0	0.51	0.64	0.51	0.50
				6.34	7.24	9.65	6.30
S2	3.30	5.94	13.0	0.66	0.72	0.79	0.70
				7.84	7.86	11.35	8.49
S3	3.30	8.50	13.0	0.71	0.74	0.82	0.73
				9.07	8.47	12.06	9.28
S4	4.30	5.14	13.0	0.71	0.75	0.87	0.75
				7.01	6.81	9.86	6.61
S5	4.30	9.30	13.0	0.79	0.78	0.90	0.78
				6.62	6.60	8.88	7.16
S6	5.30	4.44	13.0	0.81	0.78	0.92	0.77
				6.06	6.19	7.74	5.68
S7	5.30	10.00	13.0	0.88	0.84	1.08	0.96
				5.76	5.73	7.21	6.04
S8	3.30	2.44	23.5	0.57	0.67	0.61	0.59

				6.59	7.22	9.48	6.49
S9	4.30	2.44	18.5	0.65	0.75	0.70	0.63
				6.53	7.22	9.41	6.95
S10	5.30	2.44	13.5	0.79	0.82	0.90	0.85
				6.57	6.60	8.93	7.23
S13	5.30	12.00	13.5	0.85	0.81	0.89	0.91
				6.98	6.92	8.95	8.31
S14	3.30	7.22	23.5	0.66	0.76	0.75	0.65
				6.18	7.07	9.63	6.29
S15	4.30	7.22	18.5	0.76	0.86	0.91	0.86
				6.48	7.09	8.14	5.74
S16	5.30	7.22	13.5	0.88	0.83	0.81	0.96
				6.89	6.54	7.02	6.75
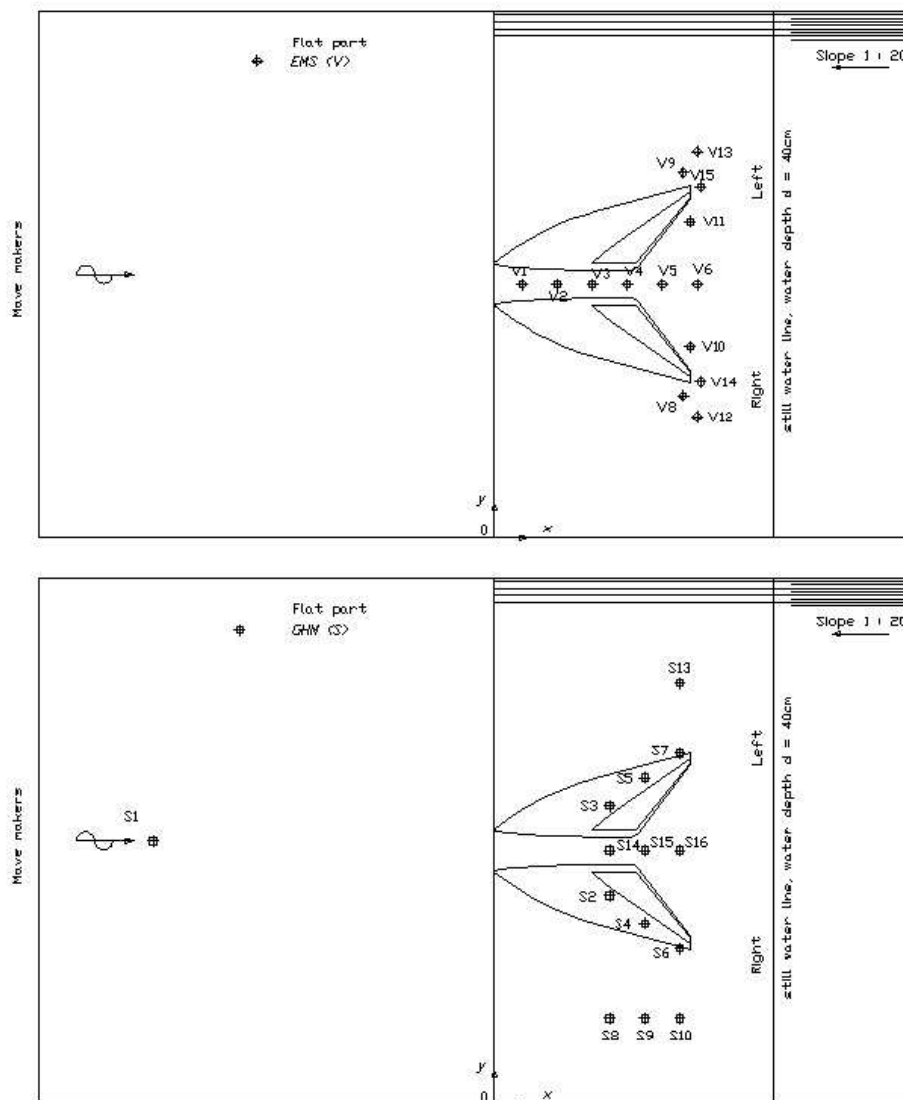
Figure B.2 – Second layout. Measurement configuration: EMS (upper panel) and GHM (lower panel).

Table B.5 – LA3_W$_{RC}$_180 - EMS position and current velocities.

Point	x [m]	y [m]	h [cm]	Velocity u / v [m/s]			
				B1	I1	M1	M2
V1	2.30	6.92	28.5	0.008	0.011	0.018	0.008
				-0.002	0.001	0.000	0.003
V2	1.80	6.92	31.0	0.007	0.012	0.029	0.008
				-0.002	0.001	-0.001	0.001
V3	2.80	6.92	26.0	0.003	0.018	0.021	0.010
				0.004	-0.007	0.003	0.005
V4	3.80	6.92	21.0	-0.104	-0.041	-0.037	-0.014
				0.117	0.023	0.039	0.032
V5	4.80	6.92	16.0	-0.173	-0.112	-0.143	-0.102
				0.044	0.103	0.185	0.135
V6	5.80	6.92	11.0	-0.155	-0.067	-0.166	-0.104
				-0.102	-0.027	-0.037	-0.101
V7	6.30	6.92	8.5	-0.090	-0.038	-0.112	-0.082
				-0.160	-0.102	-0.162	-0.196
V8	5.40	3.44	13.0	-0.092	-0.109	-0.307	-0.069
				-0.040	-0.035	-0.133	-0.019
V9	5.40	10.40	13.0	-0.140	-0.111	-0.154	-0.136
				0.115	0.119	0.201	0.068
V10	5.60	4.84	12.0	-0.196	-0.150	-0.350	-0.290
				0.012	-0.036	-0.011	0.003
V11	5.60	9.00	12.0	0.073	0.075	0.083	0.167
				-0.014	0.069	0.119	0.102
V12	5.80	2.84	11.0	-0.061	-0.073	-0.179	-0.024
				0.037	0.036	0.066	0.034
V13	5.80	11.00	11.0	-0.175	-0.146	-0.323	-0.261
				0.020	0.074	0.184	0.039
V14	5.90	3.84	10.5	-0.122	-0.114	-0.164	-0.086
				0.028	0.003	0.009	-0.007
V15	5.90	10.00	10.5	-0.103	-0.086	-0.082	-0.109
				0.056	0.096	0.271	0.137
V16	4.70	2.84	16.5	-0.045	-0.065	-0.133	-0.032
				-0.088	-0.057	-0.193	-0.029
V17	4.70	11.00	16.5	-0.145	-0.089	-0.057	-0.134
				0.080	0.054	0.034	0.049
V18	4.70	3.84	16.5	-0.073	-0.108	-0.121	-0.102
				-0.115	-0.106	-0.146	-0.062
V19	4.70	10.00	16.5	0.004	-0.002	0.009	0.011
				0.017	0.017	0.014	0.020
V20	5.30	3.84	13.0	-0.098	-0.133	-0.114	-0.133
				-0.057	-0.081	-0.102	-0.096
V21	5.30	10.00	13.0	-0.035	-0.031	-0.026	-0.017
				0.082	0.083	0.051	0.012
V22	5.90	4.84	10.5	-0.210	-0.160	-0.390	-0.233
				0.034	-0.016	0.016	0.038
V23	5.90	9.00	10.5	0.025	0.036	0.117	0.135
				-0.054	0.030	0.055	0.063
V24	3.30	3.84	23.5	0.002	-0.002	0.002	-0.027

Point	x	y	h [cm]				
				-0.010	-0.003	-0.014	-0.027
V25	3.30	10.00	23.5	0.005	0.005	-0.004	0.004
				0.022	0.000	0.015	0.013
V26	3.30	2.84	23.5	-0.004	-0.026	-0.014	-0.046
				-0.042	-0.041	-0.043	-0.038
V27	3.30	11.00	23.5	-0.015	-0.004	-0.018	-0.019
				0.026	0.007	0.025	0.014
V28	3.30	1.84	23.5	-0.010	-0.015	-0.019	-0.002
				-0.020	-0.044	-0.049	-0.069
V29	4.30	1.84	18.5	0.021	-0.003	0.022	0.030
				-0.095	-0.080	-0.178	-0.029
V30	5.30	1.84	13.5	0.047	0.001	0.061	0.016
				-0.024	0.009	-0.010	0.021
S9	3.30	12.00	23.5	-0.012	-0.021	-0.014	-0.017
				0.052	0.014	0.033	0.024
S11	4.30	12.00	18.5	-0.060	-0.090	-0.186	-0.088
				0.133	0.092	0.171	0.091
S13	5.30	12.00	13.5	-0.093	-0.100	-0.263	-0.078
				-0.031	0.043	0.115	-0.027
S14	3.30	6.92	23.5	-0.009	0.001	0.012	-0.008
				0.004	-0.005	-0.009	0.013
S15	4.30	6.92	18.5	-0.145	-0.071	-0.124	-0.083
				0.135	0.072	0.185	0.117
S16	5.30	6.92	13.5	-0.138	-0.098	-0.130	-0.109
				-0.010	0.070	0.068	0.036
S24	4.80	9.65	13.0	0.050	0.016	0.020	0.014
				0.035	0.038	0.003	0.010
S26	4.80	4.19	13.0	-0.127	-0.129	-0.148	-0.140
				-0.136	-0.127	-0.224	-0.100

Table B.6 – LA3_W$_{RC}$_180 - GHM positions and wave parameters.

Point	x	y	h [cm]	f [Hz] / H [cm]			
				B1	I1	M1	M2
S1	-9.75	7.50	40.0	0.51	0.64	0.51	0.50
				6.49	6.90	9.71	5.61
S2	3.30	5.34	13.0	0.67	0.73	0.79	0.71
				7.63	7.80	11.26	7.06
S3	3.30	8.50	13.0	0.70	0.75	0.82	0.77
				9.26	8.61	12.14	8.46
S4	4.30	4.54	13.0	0.72	0.76	0.87	0.79
				6.64	6.70	9.47	5.87
S5	4.30	9.30	13.0	0.79	0.78	0.91	0.79
				6.98	6.59	9.54	6.39
S6	5.30	3.84	13.0	0.80	0.81	0.96	0.85
				5.66	5.37	7.26	5.05
S7	5.30	10.00	13.0	0.90	0.86	1.10	0.95
				5.81	5.00	7.12	6.30
S8	3.30	2.44	23.5	0.57	0.67	0.61	0.58

				6.90	7.68	10.02	6.23
S9	3.30	12.00	23.5	0.59	0.70	0.63	0.61
				7.26	7.91	10.04	6.09
S10	4.30	2.44	18.5	0.65	0.73	0.72	0.63
				7.00	6.79	10.55	6.23
S11	4.30	12.00	18.5	0.72	0.77	0.85	0.69
				7.35	7.04	11.06	6.92
S12	5.30	2.44	13.5	0.77	0.80	0.85	0.79
				6.77	7.00	9.71	6.53
S13	5.30	12.00	13.5	0.82	0.80	0.85	0.89
				6.82	6.84	8.41	7.21
S14	3.30	6.92	23.5	0.63	0.72	0.75	0.65
				5.88	6.51	9.06	5.19
S15	4.30	6.92	18.5	0.78	0.79	0.84	0.82
				5.58	6.22	8.80	4.96
S16	5.30	6.92	13.5	0.84	0.81	0.94	0.91
				6.51	5.43	7.45	5.26
S17	3.80	3.84	21.0	0.60	0.72	0.67	0.62
				5.34	5.61	7.99	5.05
S18	3.80	2.44	21.0	0.60	0.70	0.63	0.60
				7.09	6.89	10.25	6.85
S19	4.80	2.44	16.0	0.73	0.77	0.76	0.71
				7.05	6.58	9.86	7.37
S20	3.80	2.84	21.0	0.60	0.70	0.65	0.60
				6.50	7.29	9.54	6.26
S21	4.30	13.00	18.5	0.74	0.76	0.80	0.72
				7.70	7.91	11.59	8.54
S22	3.30	1.44	23.5	0.61	0.69	0.67	0.60
				8.02	8.22	11.81	8.38
S23	4.30	1.44	18.5	0.72	0.75	0.89	0.71
				8.30	8.08	11.26	9.04
S24	4.80	9.65	13.0	0.85	0.81	1.03	0.89
				6.07	5.41	7.87	6.80
S25	3.80	4.94	13.0	0.69	0.73	0.88	0.67
				6.88	6.21	10.56	6.74
S26	4.80	4.19	13.0	0.77	0.78	0.91	0.80
				6.21	5.72	7.74	5.83
S27	3.80	8.90	13.0	0.73	0.75	0.83	0.75
				7.97	7.35	10.48	8.52
V4	3.80	6.92	21.0	0.68	0.74	0.77	0.70
				5.77	6.33	8.66	5.11
V8	5.40	3.44	13.00	0.83	0.83	0.96	0.83
				5.83	6.14	8.25	5.82
V9	5.40	10.40	13.00	0.88	0.84	1.02	0.87
				6.18	6.12	7.67	6.43
V16	4.70	2.84	16.5	0.69	0.77	0.81	0.66
				6.35	7.32	10.72	6.77
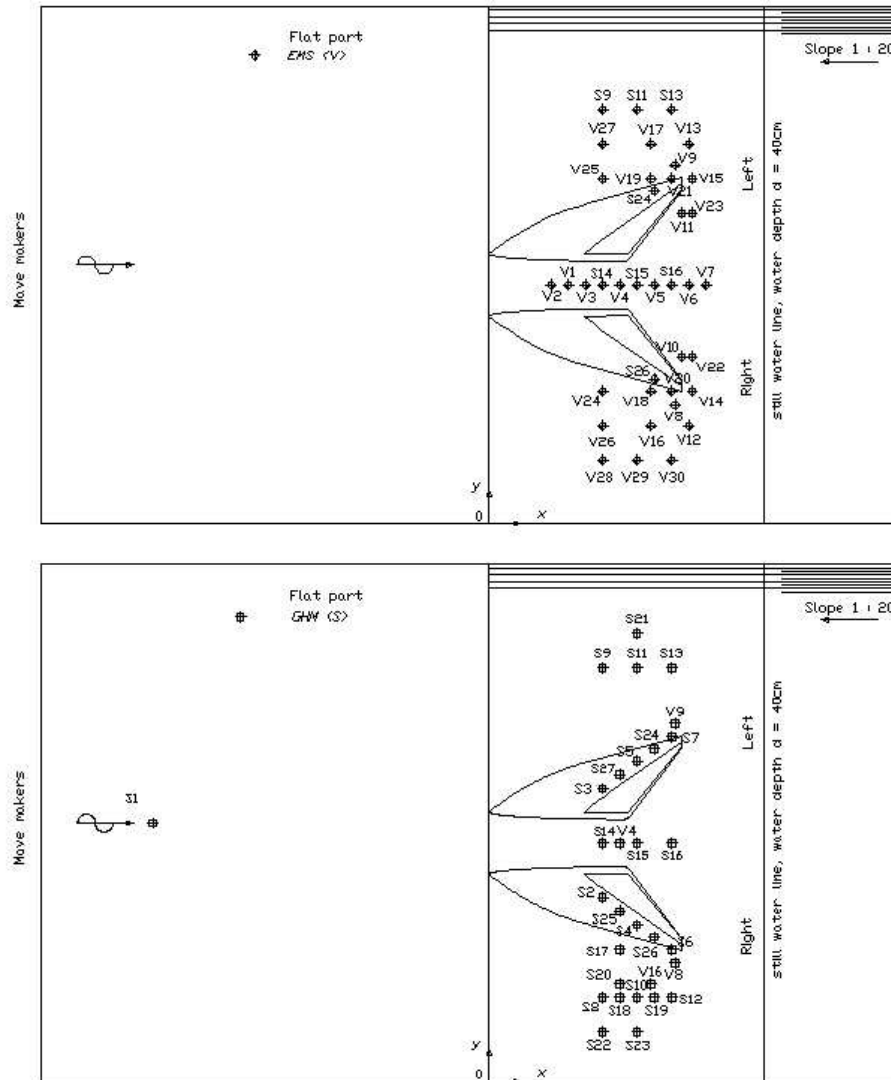
Figure B.3 – Third layout. Measurement configuration: EMS (upper panel) and GHM (lower panel).

The dispersion equation for gravity surface waves in the linear approximation:

$$\omega^2 = gk \tanh kh \qquad (C.1)$$

where $\omega = 2\pi/T$ is the angular wave frequency, $k = 2\pi/L$ is the wave number, h is the local water depth, g is the gravity acceleration.
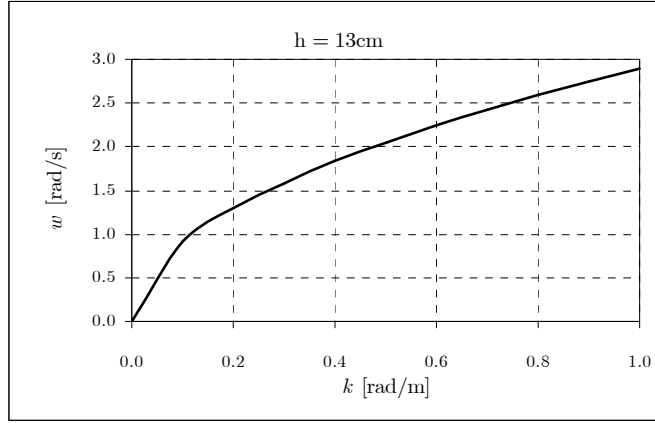
Figure C.1 – Dispersion equation.

In stationary conditions, ω is remained constant which means that change in the local water depth induces change in wave number. In the presence of a current, wave number and wave frequency are influenced. Consider the fixed reference frame (denoted with ') and the reference frame moving with the current. As the wave length is independent of the reference frame, wave numbers are the same in both cases $k = k'$, which means $k = \omega/c = \omega'/c'$. The phase speed in the fixed reference frame in the direction of the waves is $c' = c + U_\parallel$, hence:

$$\omega' = \omega + kU_\parallel \qquad (C.2)$$

For a reference frame that was moving with the mean flow (if present), the intrinsic dispersion relation is $\omega = \sqrt{gk \tanh kh}$. For a fixed reference frame in the presence of a current the general dispersion relation becomes:

$$\omega' = \sqrt{gk \tanh kh} + \vec{k}\vec{U} = \sqrt{gk \tanh kh} + kU_\parallel \qquad (C.3)$$

How the new values of wave number and wave frequency are obtained is explained with the following example. Calculation is undertaken for point S6 almost at the end of the left wave ride, water depth is 13cm, monochromatic wave M2 with the presence of an opposing current 0.164m/s. The intrinsic frequency and corresponding wave number is unknown, an iterative procedure is applied. First, the wave number is estimated:

$$k_{U_\parallel<0} \approx k_{U_\parallel=0}\left(1+2\frac{U_\parallel}{c_{\parallel=0}}\right) \qquad\qquad (C.4)$$

with $c_{U_\parallel=0}=\omega'/k_{U_\parallel=0}$ and $\varpi'=1/T'$ is the wave frequency measured at the local point S6. $k_{U_\parallel=0}$ is obtained as follows:

$$L_0=\frac{gT'^2}{2\pi}=\frac{9.81\cdot1.176^2}{2\pi}=2.161\,\mathrm{m}\Rightarrow\frac{h}{L_0}=\frac{0.13}{2.161}=0.06\,,\ \text{use Table 1 (BATTJES, 1984)}$$
to attain $kh=0.6553$ then $k=5.04$.

$$c_{U_\parallel=0}=\frac{2\pi/T'}{k_{U_\parallel=0}}=\frac{2\pi/1.176}{5.04}=1.06\quad\mathrm{m/s}\ \Rightarrow k_{U_\parallel<0}=5.04\cdot\left(1+2\frac{0.164}{1.06}\right)=6.6\quad\mathrm{rad/m}.$$
Substitute $k_{U_\parallel<0}$ in general dispersion relation:

$$\omega'=\sqrt{9.81\cdot6.6\cdot\tanh(6.6\cdot0.13)}-6.6\cdot0.164=5.628\,\mathrm{rad/s}.\ \text{Check with observation:}$$

$\varpi'=2\pi/T'=2\pi/1.176=5.34<5.628$ rad/s, try a smaller value $k_{U_\parallel,2}=6.6\cdot5.34/5.628=6.265$ rad/m $\Rightarrow\varpi'_2=5.399$ rad/s which is still larger than observed general frequency, try another smaller value of wave number until the calculated frequency is consistent with the observed value. Finally, $k=6.18$ rad/m, $\varpi'=5.34$ rad/s and $\varpi=6.34$ rad/s.
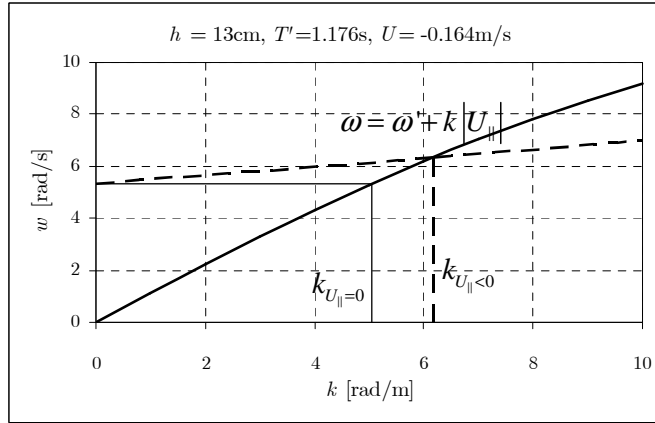
Figure C.2 – Opposing current increase intrinsic wave number and wave frequency.

Based on the new intrinsic wave number, wave length $L=2\pi/k$ is derived with a smaller value. Wave steepness consequently gets larger compared to the case of no current.